



**HAL**  
open science

## Deformation processes at the down-dip limit of the seismogenic zone: The example of Shimanto accretionary complex

Giulia Palazzin, Hugues Raimbourg, Vincent Famin, Laurent Jolivet, Y  
Kusaba, A Yamaguchi

### ► To cite this version:

Giulia Palazzin, Hugues Raimbourg, Vincent Famin, Laurent Jolivet, Y Kusaba, et al.. Deformation processes at the down-dip limit of the seismogenic zone: The example of Shimanto accretionary complex. *Tectonophysics*, 2016, 687, pp.28 - 43. 10.1016/j.tecto.2016.08.013 . hal-01383876

**HAL Id: hal-01383876**

**<https://hal.univ-reunion.fr/hal-01383876>**

Submitted on 28 Oct 2016

**HAL** is a multi-disciplinary open access archive for the deposit and dissemination of scientific research documents, whether they are published or not. The documents may come from teaching and research institutions in France or abroad, or from public or private research centers.

L'archive ouverte pluridisciplinaire **HAL**, est destinée au dépôt et à la diffusion de documents scientifiques de niveau recherche, publiés ou non, émanant des établissements d'enseignement et de recherche français ou étrangers, des laboratoires publics ou privés.

# Deformation processes at the down-dip limit of the seismogenic zone: The example of Shimanto accretionary complex

G. Palazzin <sup>a,b,c,\*</sup>, H. Raimbourg <sup>a,b,c</sup>, V. Famin <sup>d</sup>, L. Jolivet <sup>a,b,c</sup>, Y. Kusaba <sup>e,1</sup>, A. Yamaguchi <sup>f</sup>

<sup>a</sup> Univ. d'Orléans, Institut de Science de la Terre d'Orléans, UMR 7327, 45071 Orléans, France

<sup>b</sup> CNRS/INSU, Institut de Science de la Terre d'Orléans, UMR 7327, 45071 Orléans, France

<sup>c</sup> BRGM, Institut de Science de la Terre d'Orléans, UMR 7327, BP 36009, 45060 Orléans, France

<sup>d</sup> Laboratoire Géosciences Réunion - IGP, Université de la Réunion, La Réunion, France

<sup>e</sup> Department of Earth and Planetary Science, Graduate School of Science, The University of Tokyo, 7-3-1 Hongo, Bunkyo-ku, Tokyo 113-0033, Japan

<sup>f</sup> Atmosphere and Ocean Research Institute, The University of Tokyo, 5-1-5-Kashiwanoha, Kashiwa, Chiba 277-8564, Japan

## ABSTRACT

In order to constrain deformation processes close to the brittle-ductile transition in seismogenic zone, we have carried out a microstructural study in the Shimanto accretionary complex (Japan), the fossil equivalent of modern Nankai accretionary prisms. The Hyuga Tectonic Mélange was sheared along the plate interface at mean temperatures of  $245 \pm 30$  °C, as estimated by Raman spectroscopy of carbonaceous material (RSCM). It contains strongly elongated quartz ribbons, characterized by very high fluid inclusions density, as well as micro-veins of quartz. Both fluid inclusion planes and micro-veins are preferentially developed orthogonal to the stretching direction. Furthermore, crystallographic preferred orientation (CPO) of quartz *c*-axes in the ribbons has maxima parallel to the stretching direction. Recrystallization to a small grain size is restricted to rare deformation bands cutting across the ribbons. In such recrystallized quartz domains, CPO of quartz *c*-axes are orthogonal to foliation plane. The evolution of deformation micro-processes with increasing temperature can be further analyzed using the Foliated Morotsuka, a slightly higher-grade metamorphic unit ( $342 \pm 30$  °C by RSCM) from the Shimanto accretionary complex. In this unit, in contrast to Hyuga Tectonic Mélange, recrystallization of quartz veins is penetrative. CPO of quartz *c*-axes is concentrated perpendicularly to foliation plane. These variations in microstructures and quartz crystallographic fabric reflect a change in the dominant deformation mechanism with increasing temperatures: above  $\sim 300$  °C, dislocation creep is dominant and results in intense quartz dynamic recrystallization. In contrast, below  $\sim 300$  °C, quartz plasticity is not totally activated and pressure solution is the major deformation process responsible for quartz ribbons growth. In addition, the geometry of the quartz ribbons with respect to the phyllosilicate-rich shear zones shows that bulk rheology is controlled by quartz behavior. Consequently, below 300 °C, the application of quartz pressure-solution laws, based on realistic geometry derived from Hyuga microstructures, results in strongly lowering the overall strength of the plate interface with respect to the classical brittle envelop.

## 1. Introduction

As illustrated by the rheological envelopes model (e.g. Evans and Mackwell, 1995; Stöckhert and Gerya, 2005; Burov, 2011), crustal deformation is usually accounted for brittle/plastic deformation in its upper/lower part. The transition from dominant cataclastic flow to dislocation creep, often referred to as the brittle-ductile transition (Rutter, 1986; Chester, 1995) is promoted by increasing depth and temperature.

This transition is generally associated to the temperature of  $\sim 350$  °C corresponding to the limit for the onset of quartz plasticity (Tse and Rice, 1986; Hyndman et al., 1997) in quartzo-feldspatic rocks (e.g. Tullis and Yund, 1977, 1980; Blanpied et al., 1991). As observed in deformed rocks of the upper crust (Ramsay, 1967; Durney, 1972; Kerrich et al., 1977; Gratier and Gamond, 1990; Becker, 1995) above the brittle/ductile transition and in the presence of abundant intergranular fluid phase (e.g. Gratier, 1987) cataclastic flow is accompanied by the contribution of another process, pressure solution creep (PSC). PSC has been defined as a non-equilibrium process (Spiers et al., 2004; Gratier et al., 2009) involving dissolution of material at high stressed regions (e.g. grain contacts), diffusion through a grain boundary fluid phase and precipitation on grain interfaces under low normal stress (Rutter and Elliott, 1976; Raj, 1982; Spiers et al., 1990; Shimizu, 1995). The importance of PSC is also recognized at high metamorphic

\* Corresponding author at: Univ. d'Orléans, Institut de Science de la Terre d'Orléans, UMR 7327, 45071 Orléans, France.

E-mail address: giulia.palazzin@univ-orleans.fr (G. Palazzin).

<sup>1</sup> Now at Foundation for Promotion of Material Science and Technology of Japan, 1-18-6 Kitami, Setagaya-ku, Tokyo 157-0067 Japan.

conditions such as blueschist and amphibolite facies (Bell and Cuff, 1989; Wintsch and Yi, 2002), e.g. in the development of crenulation cleavage if stresses are not high enough for the activation of plastic deformation (Brander et al., 2012). The most common microstructures suggesting the operation of pressure solution are stylolite, micro-fractures, mineral shadows or fringes and dissolution cleavages (Evans, 1988; Goodwin and Wenk, 1990). In contrast with cataclasis which requires high differential stresses and act at high strain rates, pressure solution is most characteristic of slow creeping processes which take place in the upper crust at very low differential stress (Cox and Etheridge, 1989; Gratier and Gamond, 1990). Pressure solution contributes significantly to the overall strain (Ramsay, 1967; Durney, 1972; Kerrich et al., 1977; Cox and Etheridge, 1983; Gratier, 1993; den Brok, 1998; Spiers et al., 2004): the estimations of bulk volume loss due to this process can range from 30 to 80% for slaty cleavage in low metamorphic grade rocks (Wright and Henderson, 1992; Wright and Platt, 1982; Cox and Etheridge, 1983, 1989; Chester, 1995; Goldstein et al., 1995, 1998; Kawabata et al., 2007).

In the light of these considerations, the “two end-members” model describing crust rheology in terms of brittle/plastic behavior needs to be reconsidered by the integration of pressure solution creep at the transition from brittle to ductile regime (Chester, 1988, 1995; Scholz, 1988; Kirby, 1983).

The role of pressure solution is presumably highest in subduction zones, where subducted sediments deformed along the plate interface carry along a large quantity in water (Rutter and Elliott, 1976). In such setting, in order to analyze the deformation processes active near the brittle-ductile transition and the potential contribution of pressure solution, we performed microstructural and Electron Back-Scattered diffraction (EBSD) analysis on low-grade quartz-rich metasediments from the Shimanto accretionary complex (Japan). The Hyuga Tectonic Mélange is a good example for deformation at plate interface at conditions close to the brittle/ductile transition. We describe microstructural evidences of quartz deformation principally by pressure solution and crack-seal at relatively low temperatures (~250 °C) in the Hyuga Tectonic Mélange, while quartz plastic behavior is very limited. The temperature effect on the activation of quartz plasticity is then studied observing quartz microstructures from the Foliated Morotsuka, deformed at slightly higher temperatures (~340 °C). Finally, using the pressure solution creep law revisited by Gratier et al. (2009) and the geometry of naturally deformed metasediments, we discuss the implication that pressure solution creep may have for bulk rock rheology and subduction interface strength.

## 2. Geological framework

### 2.1. General structure

The Shimanto accretionary complex, exposed on-land along the Honshu, Kyushu and Shikoku islands (Fig. 1a), is recognized as an ancient accretionary prism (e.g. Taira et al., 1982, 1988). The whole complex, trending parallel to the modern trench axis of the Nankai Trough, is composed of several superposed coherent sedimentary units and tectonic mélanges, younging toward the south-east and separated from the Chichibu belt by the Butsumu Tectonic Line (BTL).

Our study focuses on the basal part of the Morotsuka Group, the Foliated Morotsuka (Raimbourg et al., 2014) and the upper part of the Hyuga Group, known as Hyuga Tectonic Mélange. The two units are juxtaposed by the Nobeoka Tectonic Line (NTL), a large-scale, low-dipping thrust fault with movement toward southeast (Murata, 1991, 1997, 1998; Saito, 1996).

### 2.2. Tectonic features

#### 2.2.1. Hyuga Tectonic Mélange

The Hyuga Tectonic Mélange, also known as Mikado Unit (Teraoka et al., 1981; Saito, 1996), is the upper member of the Hyuga group and

is exposed in the footwall of the Nobeoka Tectonic Line (Fig. 1). Microfossil assemblages indicate ages from Middle Eocene to Early Oligocene (Sakai et al., 1984; Nishi, 1988). At the outcrop scale, the Hyuga Tectonic Mélange is characterized by a typical block-in-matrix structure (e.g. Festa et al., 2010a): the coherent stratigraphic succession is disrupted and the rock is made of blocks of sandstone, siltstone breccia with minor amounts of basalt, red shales and cherts, embedded in a dark, pelitic matrix (Saito, 2008).

Estimation of the mineral composition by relative XRD peak intensity ratio of constituent minerals (Fukuchi et al., 2014) shows that quartz constitutes from 60 to 80% of the rocks of the unit, while phyllosilicates (typically chlorite and white mica) form most of the rest. A peculiar feature of the mélange rocks is the abundance of domains of precipitated quartz, on the form of veins cutting across boudinaged sandstone blocks, but also as elongated bodies within the pelitic matrix. The alignment of the broken and boudinaged sandstone blocks and quartz veins (Figs. 2 and 3) defines the foliation, which dips gently to the north-northwest (Raimbourg et al., 2014). A penetrative network of centimeter- to meter-long shear zones (Figs. 2 and 3) cut across the pre-existing foliation. Shear zones carry a lineation orientated NW-SE defined by elongated blocks and phyllosilicates. Their kinematics has systematically top-to-the-SE sense of shear.

From petrological analysis of basalts blocks, the syn-deformational metamorphic conditions are within the prehnite-pumpellyite facies (Imai et al., 1971; Toriumi and Teruya, 1988). Peak temperatures estimated with illite crystallinity (Hara and Kimura, 2008; Mukoyoshi et al., 2009) and vitrinite reflectance (Kondo et al., 2005; Mukoyoshi et al., 2009) range between ~250–280 °C. Raimbourg et al. (2015) find similar temperatures by microthermometry on fluid inclusions.

#### 2.2.2. Foliated Morotsuka

The Foliated Morotsuka corresponds to the basal portion of the Morotsuka Group and form the hanging wall of the NTL along most of its length (Fig. 1). Ages, estimated by microfossil assemblages, indicate depositional lapse in the Cenomanian to Campanian/Maastrichtian (Teraoka and Okumura, 1992).

The Foliated Morotsuka has sometimes been described as a tectonic mélange characterized by sandstone blocks and pillow basalts embedded in pelitic matrix (Teraoka and Okumura, 1992; Saito, 1996), but in most areas blocks are rare and the unit is composed simply of fine alternations of quartz-rich and phyllosilicate-rich layers defining a metamorphic foliation (Fig. 4).

In the studied area, the metamorphic foliation gently dips to the NW. On the foliation planes, the well-developed lineation is marked by the alignment of white mica and chlorite crystals. Deformation kinematic is principally vertical shortening associated with coaxial stretching to the NNW-SSE, with a minor contribution of top-to-the-NNW shear zones (Fabbri et al., 1990; Raimbourg et al., 2014). Centimeter-to-meter long quartz veins (Fig. 4) are distributed throughout the whole unit and flattened in the foliation.

Metamorphic conditions have been estimated to prehnite-pumpellyite to greenschist facies (Toriumi and Teruya, 1988), in agreement with paleotemperatures derived from illite crystallinity (300–310 °C) (Hara and Kimura, 2008) and vitrinite reflectance (320 °C) (Kondo et al., 2005).

### 2.3. Tectonic interpretation of the deformation

A general scheme of evolution of the Shimanto accretionary complex is developed in detail in (Raimbourg et al., 2014). We recall here the principal results regarding the tectonic interpretations of the deformation recorded in the two units considered here. (1) The foliation of the base of the Morotsuka Group developed at Eocene time after it had already been accreted to the hanging wall of the plate interface. It occurred near the plate interface as a result of an event of prism collapse and horizontal extension (Fig. 1b).

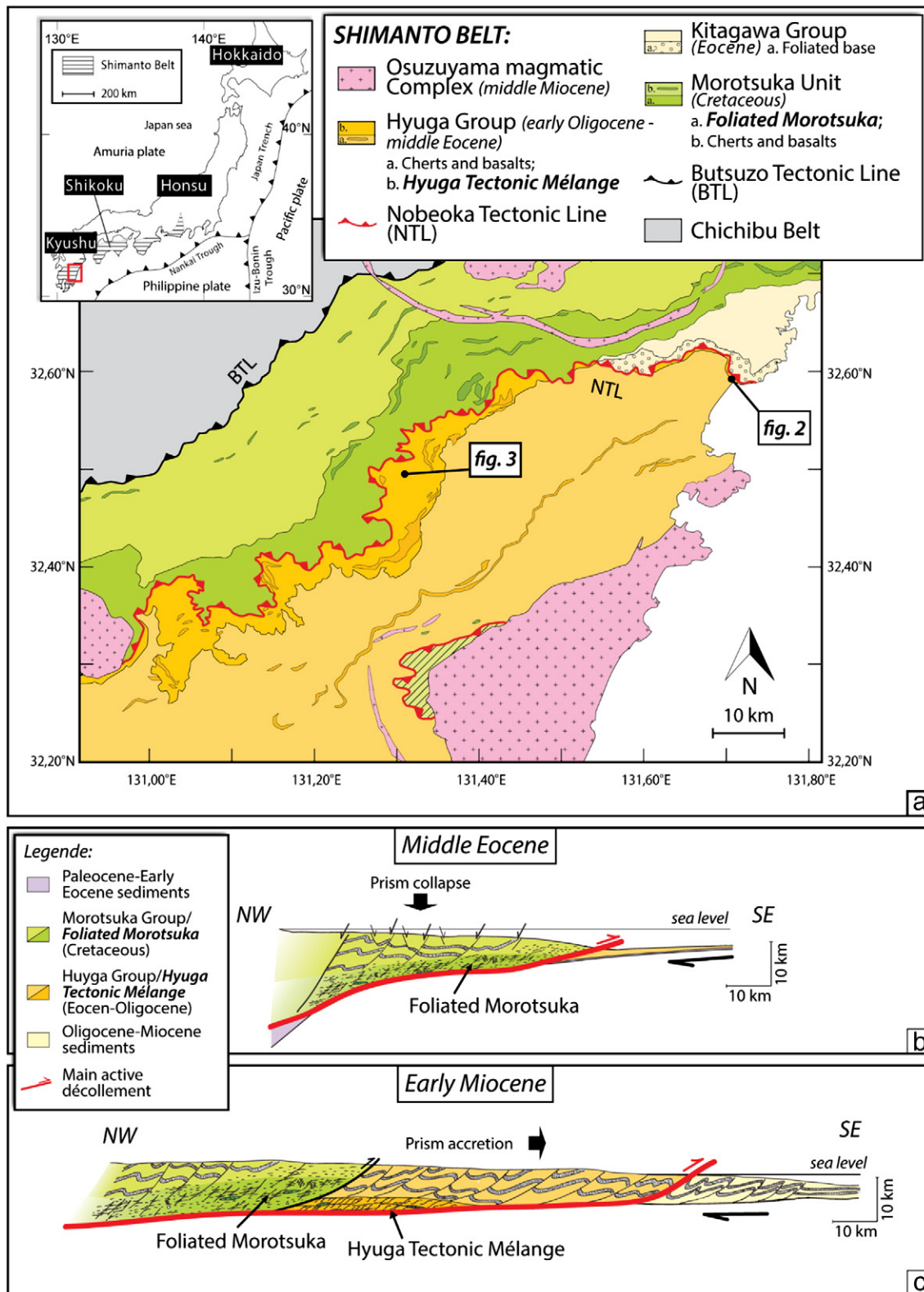


**Fig. 1.** a) Simplified geological map of the Shimanto accretionary complex on Kyushu Island (from Murata, 1997). Simplified reconstructions of the Belt evolution, showing the tectonic interpretations (in b and c) of the deformation recorded in the base of Morotsuka group and Hyuga Tectonic Mélange, respectively (modified from Raimbourg et al., 2014). b) Middle Eocene prism collapse, associated with a penetrative horizontal extension and vertical shortening in the foliated base of the Morostuka Group. c) Sometimes in Early Miocene time lapse, the Hyuga Tectonic Mélange is strongly sheared along the plate interface and underplated at the base of the prism.

(2) The deformation of the Hyuga Tectonic Mélange occurred sometimes in the time lapse Early Oligocene–Early Miocene, along the plate interface, as a result of subduction-related shearing and underplating of the unit (Fig. 1c). This interpretation implies that

both unit recorded a single stage of deformation, although at a different time and with different kinematics. Fig. 1c represents the position of the two domains of interest before the slip on the NTL in Middle Miocene.



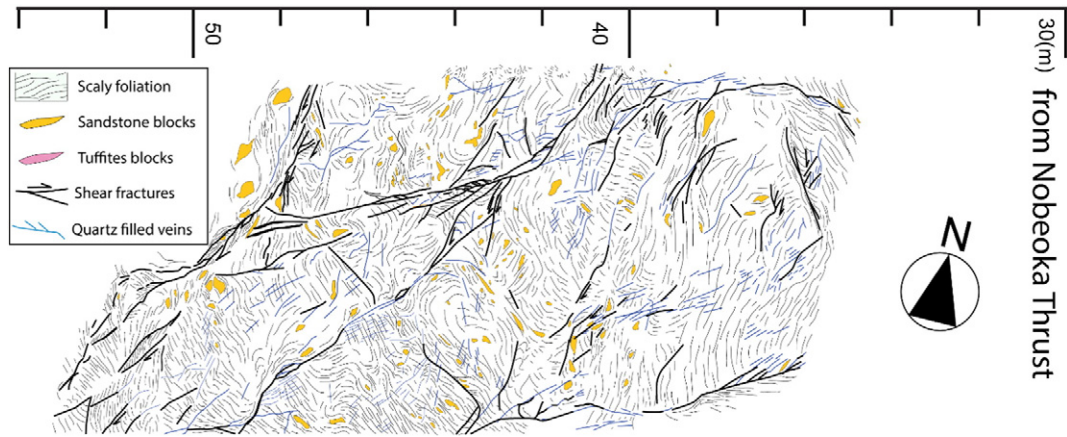


Fig. 2. Exposure of the Hyuga Tectonic Mélange along the eastern coast of Kyushu, in the vicinity of the NTL (location in Fig. 1a).

### 3. Analytical methods

#### 3.1. Rock sample preparation

All rock samples were cut orthogonally to the foliation (XZ-plane) to obtain polished thin sections of about 30  $\mu\text{m}$  thickness for standard petrographic observations, EBSD and Raman Spectroscopy of Carbonaceous

Material (RSCM) analyses. Double-polished thick sections of about 150  $\mu\text{m}$  were prepared for Fourier Transform Infra-Red (FTIR) analyses.

#### 3.2. Raman spectroscopy of carbonaceous materials

RSCM is an alternative method to classical vitrinite reflectance (VR) and illite crystallinity (IC) to constraint paleo-temperatures of rocks.

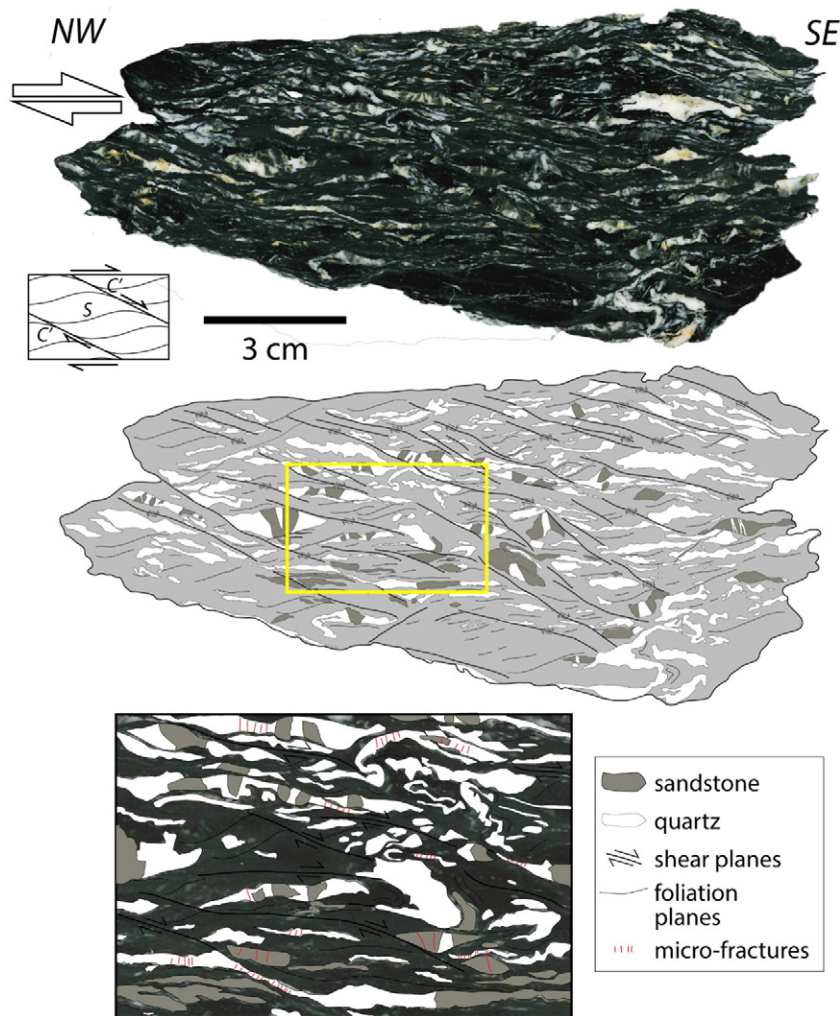


Fig. 3. Sketch of a macroscopic slice of sample of Hyuga Tectonic Mélange, with the block-in-matrix structures. Blocks are made of sandstone boudins or abundant, elongated domains of precipitated quartz. Sandstones blocks and quartz domains are both boudinaged, folded and deformed by top-to-SE shear zones. Most shear zone has a finite length and terminates on sandstone/quartz bodies. Location in Fig. 1a.

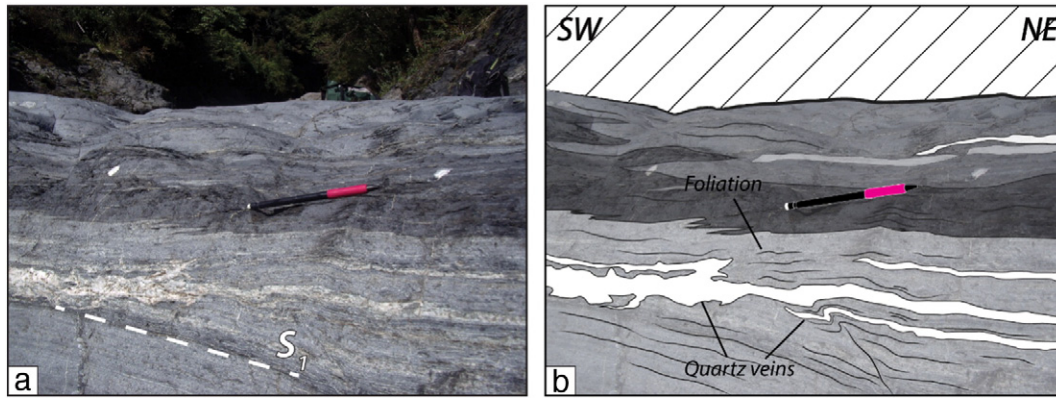


Fig. 4. Foliated Morotsuka outcrop, showing quartz veins flattened in the foliation.

The RSCM method studies the evolution of Raman spectral bands of the carbonaceous material. It has been calibrated for medium to high metamorphic grade by *Beysac et al. (2002)* and more recently for low grade metamorphic rock by *Lahfid et al. (2010)*. In this study, we applied the calibration proposed by *Lahfid et al. (2010)* in the range of 200–350 °C to estimate paleo-temperatures Hyuga Tectonic Mélange and of Foliated Morotsuka.

Raman analyses were performed using a confocal Raman Renishaw InVia Reflex micro-spectrometer at BRGM, Orléans. Before each session, the micro-spectrometer was calibrated with silicon standard. The light source was a 514.5 nm argon laser focused by a Leica DM2500

microscope with a 100× magnification objective. The laser power at the sample surface was about 1 mV. After several filtering steps, the signal was finally analyzed by a CCD NIR/UV detector. Sets of 10 to 15 spectra were measured for each sample on polished thin sections. To avoid the effect of polishing on the CM structural state, we analyzed CM particles a few microns below the thin section polished surface.

### 3.3. Crystallographic preferred orientation

EBSD was employed to map the crystallographic preferred orientation (CPO) of the samples. Thin sections were previously chemically

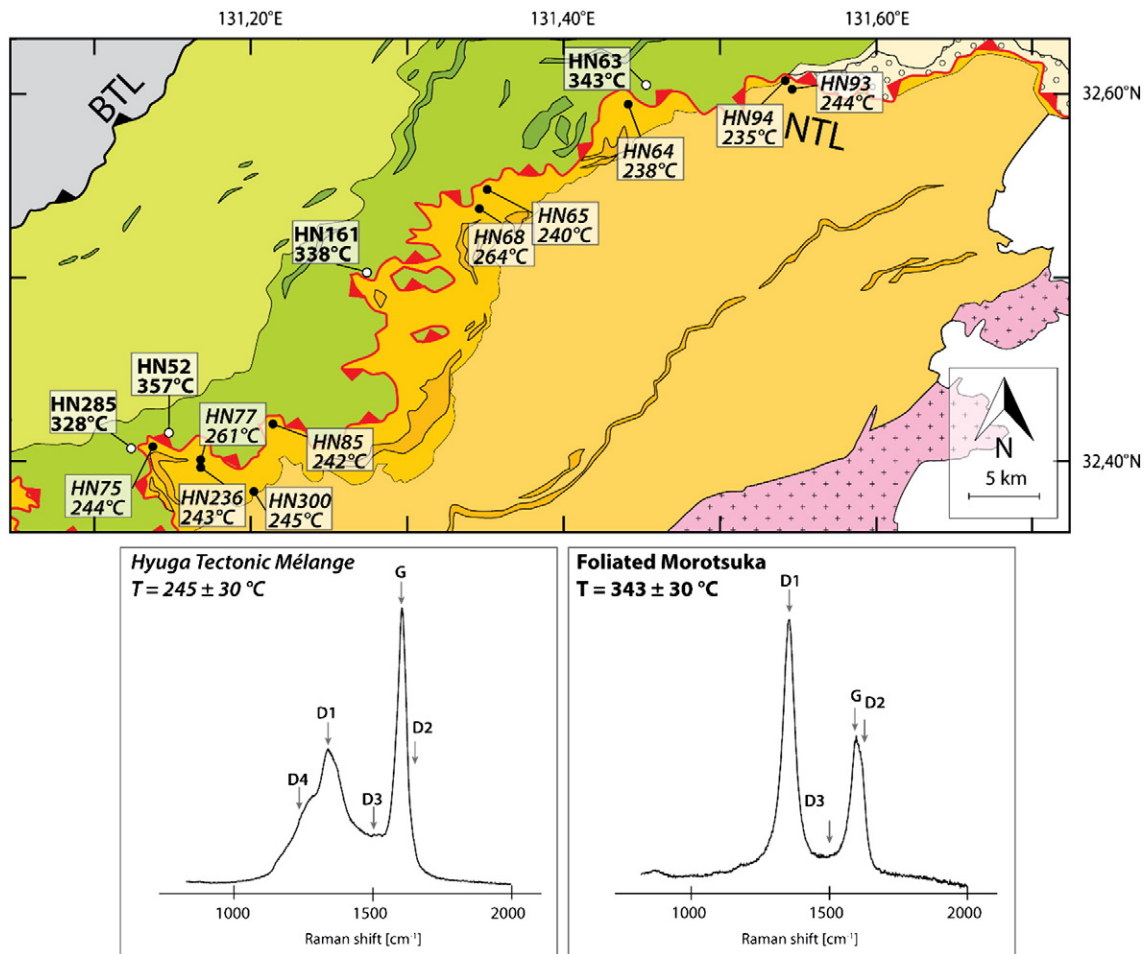


Fig. 5. Paleo-temperatures map of the studied area derived from Raman Spectroscopy of Carbonaceous Material and two examples of spectra associated to the two units. Italic titles/black dots indicate temperatures for Hyuga Tectonic Mélange while bold titles/white dots are employed for Foliated Morotsuka data. Colors refer to the legend in Fig. 1. GPS coordinates for each sample are listed in Table 1.



**Table 1**

Peak-temperatures derived from Raman Spectroscopy of Carbonaceous Material for the Hyuga Tectonic Mélange (HTM) and the Foliated Morotsuka (FM). Raman parameter is defined as ratio of the areas of the measured peaks:  $(D1 + D4)/(D1 + D2 + D3 + D4 + G)$  area ratio (Lahfid et al., 2010). SD is standard deviation.

Sample	Longitude (°)	Latitude (°)	Unit	Number of analyses	Raman parameter	T mean [°C]	SD
HN 52	131,24250	32,41610	FM	10	6,63E-01	357	22
HN 63	131,47757	32,60295	FM	9	6,52E-01	343	8
HN 64	131,46297	32,59442	HTM	9	5,65E-01	238	5
HN 65	131,40357	32,54517	HTM	10	5,67E-01	240	6
HN 68	131,39924	32,54939	HTM	10	5,87E-01	264	22
HN 75	131,17177	32,40026	HTM	10	5,59E-01	244	10
HN 77	131,24460	32,41619	HTM	10	5,85E-01	261	27
HN 85	131,31481	32,42867	HTM	10	5,69E-01	242	11
HN 91	131,24250	32,41610	HTM	10	5,61E-01	233	8
HN 93	131,58203	32,60445	HTM	10	5,70E-01	244	16
HN 94	131,57563	32,60837	HTM	10	5,63E-01	235	12
HN 181	131,35247	32,50364	FM	13	6,48E-01	338	20
HN 285	131,23915	32,42005	FM	12	6,40E-01	329	27
HN 236	131,25534	32,40831	HTM	15	5,70E-01	243	23
HN 300	131,27903	32,40331	HTM	14	5,72E-01	245	5

polished with a colloidal silica suspension (0.04  $\mu\text{m}$  Colloidal silica suspension by Struers) and then carbon-coated to prevent charging effects. All thin sections were tilted of  $70^\circ$  to the electron beam to produce clear diffraction patterns. Data were collected using an EDAX PEGASUS EDS/EBSD system and OIM DC 6.4 software (manufacturer EDAX, Mahwah-USA) at the BRGM of Orléans, France. The working distance was of about 20 mm, at an accelerating voltage of 25 kV. Crystallographic Preferred Orientations were collected using a step size  $<2 \mu\text{m}$  in order

to sample a wide range of size of grains. Data were then processed to produce orientation charts and pole figures (PF) based on 'one-point-per-grain' analysis. This system allows assigning a similar weight to all grains separated by misorientation boundaries  $>10^\circ$ , independently of their size. Inverse pole figures map (IPF) are color-coded in agreement with the corresponding color key. Grain sizes estimations were derived from grain boundaries drawn manually from the superposition of image quality (IQ) and unique color grain (UCG) maps (maps obtained from EBSD analyses). In stereographic plots, X and Z directions correspond to kinematics directions, i.e. stretching direction and pole to foliation, respectively.

### 3.4. IR measurements

Infrared microspectroscopy is an analytical technique that allows quantifying water content in rocks. The analyses were conducted on different quartz microstructures belonging to Hyuga Tectonic Mélange and Foliated Morotsuka in order to investigate differences in water content/speciation associated to textural variation. After preparing double polished thick sections, the chosen microstructure was pre-cut by a circular micro-saw. Then the pre-cut zones were removed from the glass slides by immersion in acetone: this operation dissolves the cyanoacrylate adhesive employed to prepare sections. Each sample was put on a NaCl stage upon a stainless steel plate with a hole and then analyzed with a Nicolet Continuum FT-IR Microscope, using a  $32\times$  objective. Water amount in quartz grains was measured with a microscopic FTIR spectrometer (Nicolet-6700 FT-IR Thermo Scientific). All spectra were obtained by collecting 128 scans with a spectral range from  $4000$  to  $1500 \text{ cm}^{-1}$  and at a  $4 \text{ cm}^{-1}$  resolution. A background (B) was measured for the aperture area without the sample; then a sample transmission spectrum (S) was measured on the desired position of the sample. A final absorption spectrum was obtained by taking absorbance Abs

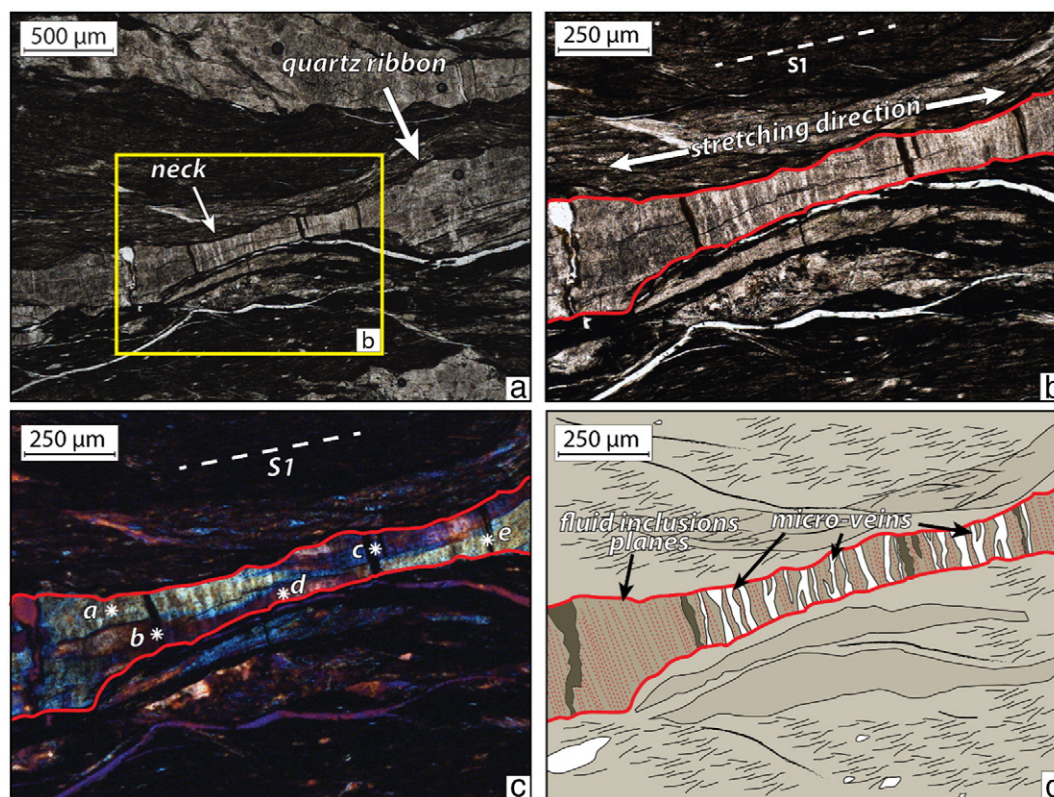


**Fig. 6.** a–b–c) Microphotographs of Hyuga Tectonic Mélange quartz ribbons, showing the structure of elongated necks parallel to the stretching lineation. The quartz ribbon is composed of several elongated quartz crystals, apparent through their different interference colors here indicated by the asterisk and a letter. d) Interpretation of b): the neck in the quartz ribbon is filled by multiple micro-fractures, fluid inclusions trails (red dotted lines) and veins (thick white veins), aligned perpendicularly to the main stretching direction. a–b) Optical microscope transmitted light, c) with cross nicols.

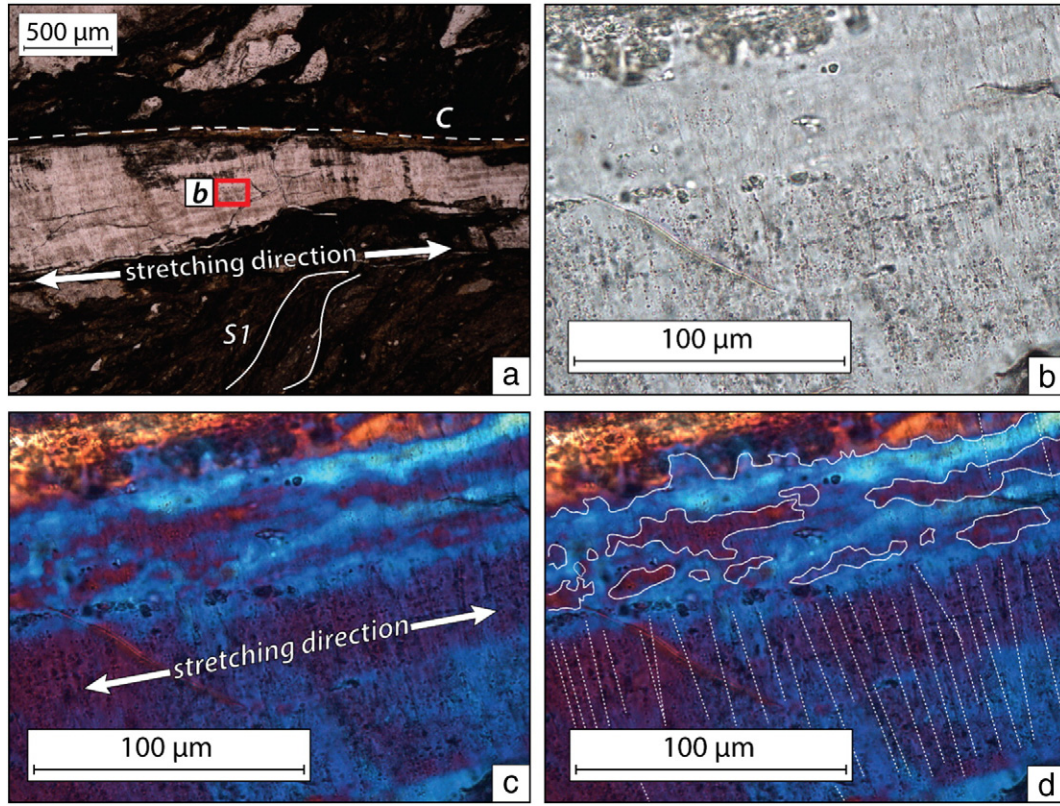


**Fig. 7.** Internal structure of a quartz ribbon elongated along a shear plane ( $c'$ ). The distribution of fluid inclusions is very heterogeneous: the upper part of quartz (panels a and b) is depleted in fluid inclusions contrarily to the lower part. In the depleted domain, sutured boundaries, called “saw-tooth” boundaries, are apparent (panel c and interpretative sketch in panel d). In the fluid inclusion-rich domain, most of the inclusions align along planes perpendicular to the stretching lineation. a–b) Optical microscope transmitted light, c) with cross nicols and wave plate.

( $Abs = -\log_{10} B/S$ ) as a function of the wavenumber ( $\text{cm}^{-1}$ ). All spectra were processed with this baseline correction. The water amount in quartz was determined by the height of the absorbance peak at  $3400 \text{ cm}^{-1}$  (Fig. 5) considered to be due mainly to the molecular water ( $\text{H}_2\text{O}$ ) in fluid inclusions contained in quartz (Aines and Rossman, 1984; Kronenberg and Tullis, 1984; Kronenberg et al., 1990a). According to the Lambert–Beer’s law,  $A$  is proportional to the water concentration in a sample  $C$  ( $\text{H}:10^6 \text{ Si}$ ) and the sample thickness  $d$  (cm):

$$A = \epsilon C d \quad (1)$$

where  $\epsilon$  ( $\text{L mol}^{-1} \text{ cm}^{-2}$ ) is the molar absorption coefficient, assumed to be 0.81 (Kats, 1962). Then, the molar concentrations of  $\text{H}:10^6 \text{ Si}$ , has been converted to weight ppm by using the relation 1 ppm  $\text{H}_2\text{O}$  to  $\text{SiO}_2$  by weight is equal to  $6.67\text{H}:10^6 \text{ Si}$ .

The largest source of error in the water amount estimation lies in the measurement of the sample thickness  $d$  ( $\sim 150 \mu\text{m}$ ). This value can be obtained by microscope or by measuring the height of the peak at  $1790 \text{ cm}^{-1}$  making use of Lambert–Beer’s Law. To allow the estimated water concentration to be compared to the results of previous studies on quartz (e.g., Kronenberg et al., 1990b; Kronenberg and Wolf, 1990; Post and Tullis, 1998), we also used the calibration proposed by Paterson (1982), based on the integral of absorption coefficient as:

$$C = \frac{1}{d} \frac{1}{I_{\text{eff}}} \int K(\nu) d\nu \quad (2)$$

where  $d$  (cm) is the thickness of the sample,  $K$  is the absorption coefficient,  $\nu$  ( $\text{cm}^{-1}$ ) is the wavenumber and  $I_{\text{eff}}$  ( $\text{cm}^{-2}$  per mol  $\text{H}/\text{l}$  of quartz) is the effective integral molar absorption coefficient. Values of  $I_{\text{eff}}$  vary according to the concentration in  $\text{H}$  and we made the calculations with a value of  $27,000 \text{ cm}^{-2}$  corresponding to concentrations of  $4,000 \text{ H}/10^6 \text{ Si}$ .

## 4. Results

### 4.1. Raman spectroscopy of carbonaceous material

The estimated peak temperatures for Hyuga Tectonic Mélange and Foliated Morotsuka by RSCM are  $244 \pm 30 \text{ }^\circ\text{C}$  and  $342 \pm 30 \text{ }^\circ\text{C}$  and, respectively. These values are in good agreement with previously estimated peak temperatures with illite crystallinity (IC) and vitrinite reflectance (VR) (e.g. Kondo et al., 2005) techniques for the Hyuga Tectonic Mélange. For Foliated Morotsuka,  $\sim 40 \text{ }^\circ\text{C}$  difference is observed between these results and the measurement proposed by Mukoyoshi et al. (2009) by vitrinite reflectance. Data are presented in Table 1 and the corresponding samples locations are reported in Fig. 5.

### 4.2. Microstructural description

#### 4.2.1. Hyuga Tectonic Mélange

At the micro-scale, foliation planes are defined by fine-grained phyllosilicates (mostly chlorite), which form wavy surfaces through the matrix, and that wrap around sandstone blocks and quartz veins (Figs. 3 and 6). Spacing between cleavage planes varies from  $< 10 \mu\text{m}$  to several tens of micrometers and its density increase in areas where blocks/veins are close to each other. Many quartz ribbons are found in the matrix (Figs. 6 and 7a), displaying a high density of micro-veins and fluid inclusions (Fig. 6b and d), giving a dusty color to the quartz. Fluids inclusions tend to be arranged in a dense network of planar trails preferentially orientated perpendicularly to the major axis of ribbons, i.e. to the main stretching direction (Figs. 6b and d and 7). Fluid inclusions trails and micro-veins are particularly abundant in thinned domains of the ribbons (“neck” in Fig. 6).

Ribbons are composed by several elongated, superposed quartz crystals of several hundred micrometers of length (Fig. 6c). The



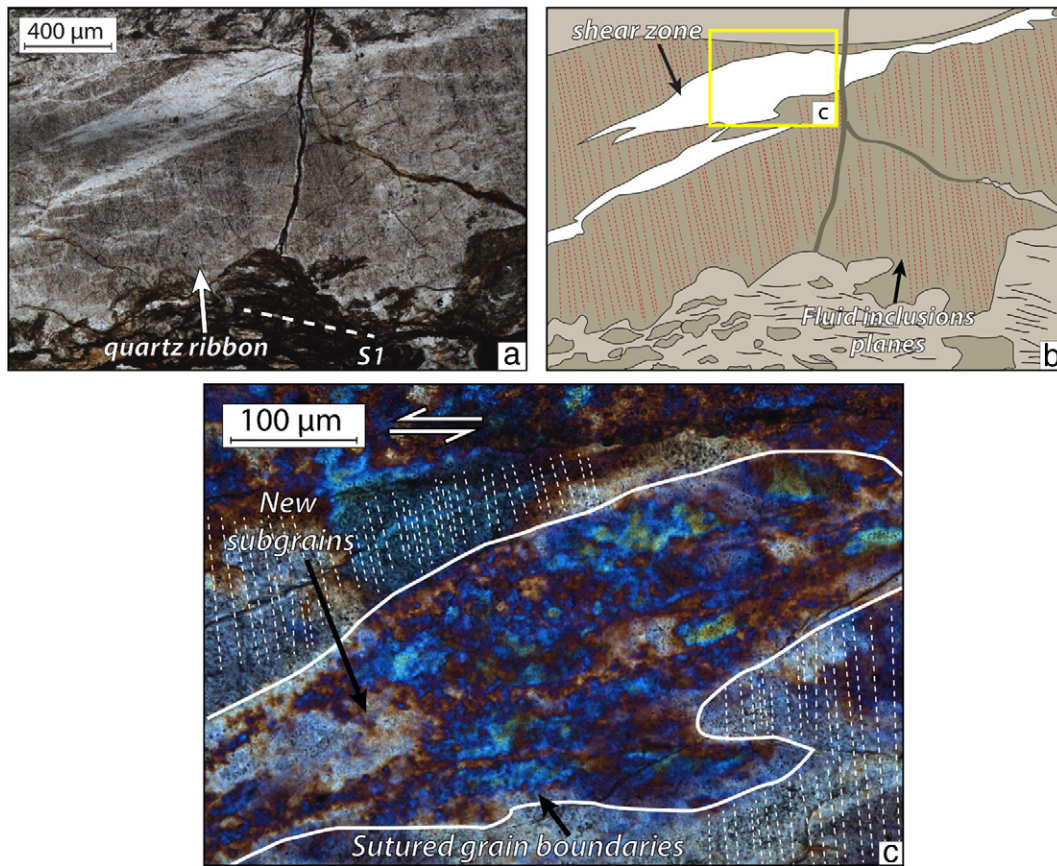


**Fig. 8.** a–b) Shear band cutting across a quartz ribbon. The shear band is characterized by a low density in fluid inclusions with respect to the surrounding quartz, apparent in the color contrast. Grain size reduction is observed inside the shear band. The small grains are characterized by sutured boundaries. a) Optical microscope transmitted light, b) with cross nicols and wave plate.

superposed crystals are delimited by boundaries which can vary from slightly curved to sutured, comparable to the “saw-tooth” grain contacts described by Fagereng et al. (2010) (Fig. 7c and d). Domains where boundaries are sutured are depleted in fluid inclusions (Fig. 7b). Undulose extinction is commonly observed along quartz ribbons as well as the presence of local small bulges (Fig. 7d).

Narrow shear zones cutting across quartz ribbons are also observed (Fig. 8). Shear zones are characterized by strong decrease in fluid inclusion density with respect to the surrounding material (Fig. 8a and b) associated to an important grain size reduction (Fig. 8c). Inside these deformation bands, new bulging inside relict grains as well as sutured grain boundaries bonding small grains are observed.

#### 4.2.2. Foliated Morotsuka

The fine-grained phyllitic matrix (Fig. 9a) is deformed through the development of a metamorphic foliation. Pressure solution is evidenced by the frequent strain shadows next to pyrite grains. The large number of quartz veins cutting across the matrix have flattened almost parallel to the cleavage planes (Fig. 9a). Within the deformed veins, large relict porphyroclasts (between 250 μm and 1 mm size) display undulose extinction and elongated ‘blocky’ subgrains (Fig. 9b). Domains of small (5 to 10 μm) recrystallized grains develop around large relict porphyroclasts elongated parallel to the stretching direction. Bulged inlets are frequently observed between crystals as well as equant recrystallized grains which decorate porphyroclasts rims (Fig. 9c). The grain boundary at the limit between relict and recrystallized domains is strongly sutured (Fig. 9d).

### 4.3. Crystallographic preferred orientation

#### 4.3.1. Hyuga Tectonic Mélange

Quartz ribbons display quite strong *c*-axes CPO with a well-defined maximum in the X-direction (stretching direction) (Fig. 10). Inverse pole figure of the X direction show the strong preferred orientation of quartz crystals: the dominant colors are red to orange. Crystal boundaries have two dominant orientations: they are preferentially orientated perpendicular (Fig. 10d) or parallel (Fig. 10e) to the stretching direction.

In contrast to quartz ribbons, quartz CPO in shear bands accompanied by grain size reduction (Fig. 11) display a cluster of *c*-axes nearly perpendicular to the foliation and to the shear zone boundaries (Fig. 11b).

#### 4.3.2. Foliated Morotsuka

In this unit, all studied samples show a weak CPO, as attested by the large range in grain color in IPF Map (Fig. 12a). The CPO is nevertheless systematic: *c*-axes cluster are generally at a small angle to Z-axis (Fig. 12b). Relict crystals (Fig. 12c) show lobate external rims as well as internal variations in crystal orientation defining subgrains of size ~10 μm. These domains are counteracted by low angle misorientation boundaries.

### 4.4. Intra-crystalline water content

Four different microstructures have been analyzed: the quartz ribbons and the shear bands in the Hyuga Tectonic Mélange, the relict and the recrystallized quartz grains in Morotsuka unit. All the IR spectra have a broad band around 3400 cm<sup>-1</sup> characteristic for molecular water



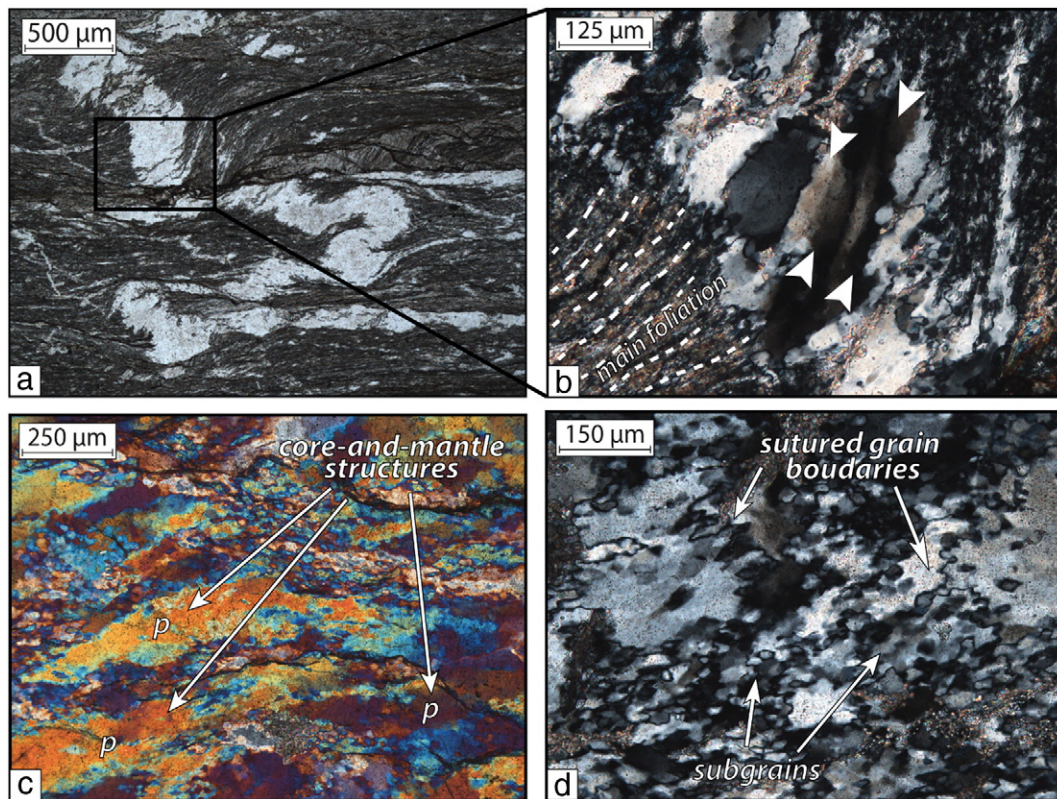


**Fig. 9.** Example of microstructures observed in the Foliated Morotsuka. a–b) Folded, flattened and partly sheared quartz vein. b) Elongated subgrains (indicated by white arrows) develop within the deformed quartz grains. c) Core-and-mantle structures defined by domains of small, recrystallized grains surrounding large, relict porphyroclasts (“p”) elongated parallel to the foliation. d) Sutured grain boundaries between recrystallized and relict domains of quartz. a–b–d) Optical microscope transmitted light, c) with cross nicols and wave plate.

(Aines and Rossman, 1984). A typical IR spectrum of this study is shown in Fig. 13, in this case a spectrum inside a quartz ribbon in the Hyuga Tectonic Mélange and for recrystallized grains in the Morotsuka unit. A broad absorption band representing O–H stretching vibration is observed around  $3400\text{ cm}^{-1}$ . Seven peaks, characteristic of quartz, were observed from  $2000$  to  $1400\text{ cm}^{-1}$  ( $1990$ ,  $1870$ ,  $1790$ ,  $1680$ ,  $1610$ ,  $1524$ ,  $1490\text{ cm}^{-1}$ ) due to overtone and combination modes of Si–O vibrations (Ito and Nakashima, 2002).

The concentration in “liquid-like” water is at first order controlled by the density of fluid inclusions. In Hyuga, the larger quantities have been found for quartz ribbons, with mean values of  $\sim 20,000\text{ H}/10^6\text{ Si}$ , while shear bands with recrystallized grains, poorer in fluid inclusions, show a lower amount  $\sim 13,000\text{ H}/10^6\text{ Si}$ . In Foliated Morotsuka, the cores of relict grains show water amounts of  $\sim 17,500\text{ H}/10^6\text{ Si}$ , whereas surrounding recrystallized grains, poorer in fluid inclusions, have a much lower water content ( $\sim 3,000\text{ H}/10^6\text{ Si}$ ). Note that the values in recrystallized grains incorporate, in addition to the water within the grain interiors, the contribution of water along the grain boundary, because recrystallized grain size (see Table 2) is smaller than the FTIR window aperture ( $50 \times 50\text{ }\mu\text{m}^2$ ). There is therefore a clear decrease in water content resulting from recrystallization. This decrease is associated with the “annealing” of pre-existing fluid inclusions during recrystallization, possibly as a result of extensive grain boundary migration.

## 5. Discussion

### 5.1. Deformation mechanisms

#### 5.1.1. Hyuga Tectonic Mélange

The elongated crystals constituting the quartz ribbons have a composite internal structure, made of a succession of bands perpendicular to the stretching direction (Figs. 6b–d and 10e). Some of these bands are clearly recognized as veins, while a smaller set of veins is attested

by fluid inclusions planes also perpendicular to the stretching direction. The growth of the elongated crystals in the ribbons is therefore the result of repetitive cycles of fracturing and fracture-filling. The large water amount measured in quartz ribbons by FT-IR is thus directly related to crack-healing. An analogue of quartz ribbons could be the “shear or bedding veins”, commonly found in low grade deformed meta-sedimentary rocks (Cox, 1987; Labaume et al., 1991; Cosgrove, 1993; Le Hebel et al., 2002; Fagereng et al., 2010, 2011). The strong CPO, with c-axes parallel to the main stretching direction, developed as only favorably oriented crystals grew by this cyclic process. Similar crystallographic fabrics are reported in literature for low metamorphic grade rocks by Cox and Etheridge (1983); Hippertt (1994); Becker (1995); Stallard and Shelley (1995). The authors associated the c-axes X-maximum to crystal growth in response to pressure solution. The observed microstructures are thus comparable to slickenside fibers developed along shear planes during shear. The source of the new deposited crystalline material is inferred to be the quartz fraction dissolved along foliation surfaces from the surrounding clay matrix. The foliation planes, pervasively distributed in the whole rock, are perpendicular to tensile microfracturing associated to quartz ribbons. Foliation planes (dissolution sites) and ribbons (precipitation sites) can thus be associated to deformation by pressure solution.

We also observed some evidences for the activation of quartz recrystallization inside shear bands cutting across porphyroclasts, with a large grain size decrease down to  $\sim 10\text{ }\mu\text{m}$ . The associated CPO is indicative of the activation of the basal slip system in the  $\langle a \rangle$  direction (Schmid and Casey, 1986). Recrystallized grains are bonded by sutured grain boundaries, suggesting that recrystallization is promoted by the mobility of grain boundaries. These shear zones contains much lower fluid inclusions than the undeformed surrounding porphyroclasts (Fig. 8a–b), thus grain boundaries motion may also be responsible for water (i.e. fluid inclusion) expulsion.



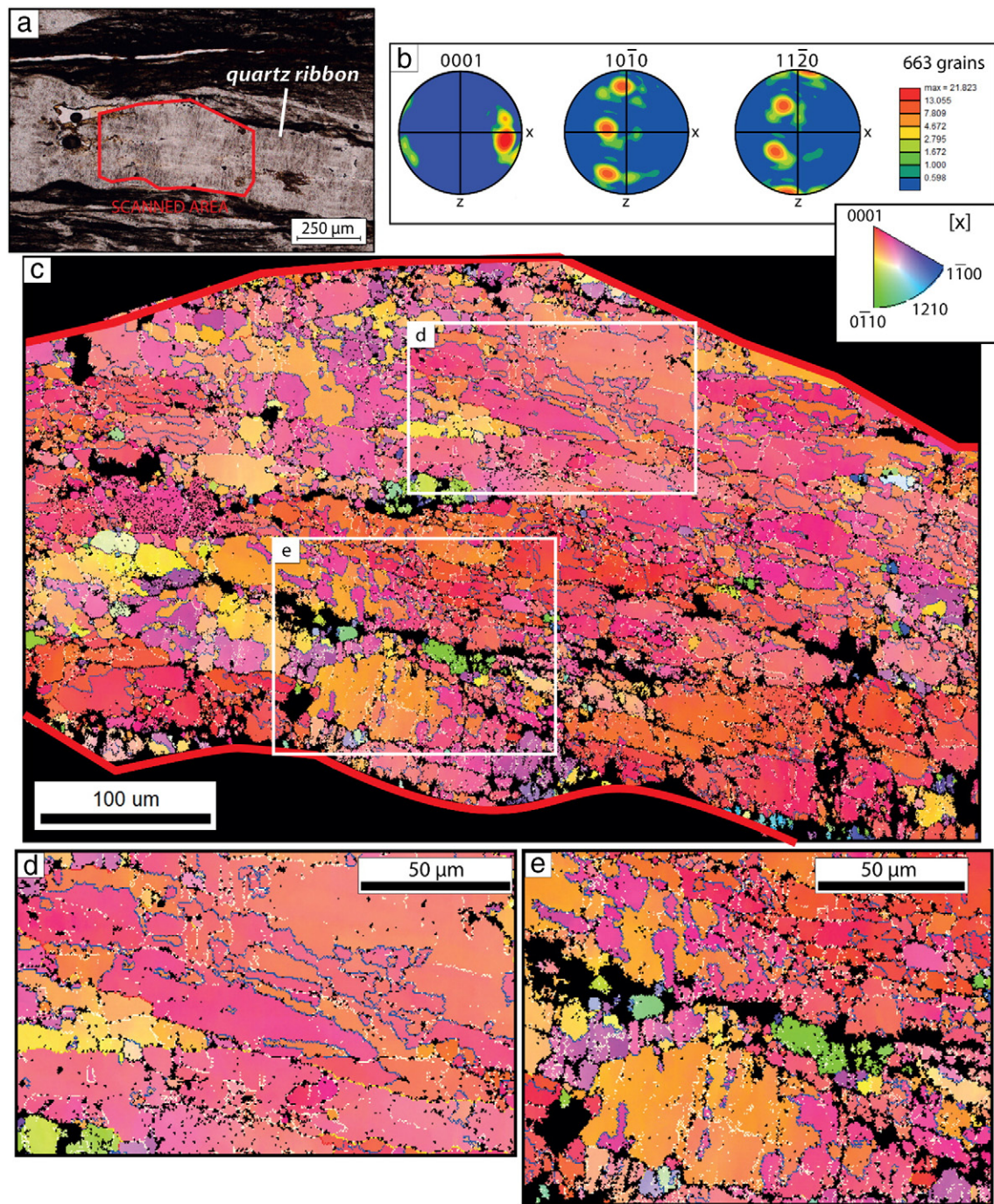


**Fig. 10.** Quartz crystallographic fabrics in a ribbon in the Hyuga Tectonic Mélange. a) Optical microscope image of the scanned area. b) Lower hemisphere pole figure of  $c$  (0001) and  $a$  ( $10\bar{1}0$ ) axes and  $m$  ( $11\bar{2}0$ )-planes.  $c$ -axis distribution has a strong maximum parallel to the stretching lineation (X direction). c–d–e) EBSD map of the ribbon (with a color code associated to inverse pole figure of X direction), showing a net preferred orientation of  $c$ -axes in the X-direction. d) Quartz domains developed parallel to the main stretching direction are interpreted as the equivalent of “saw-tooth” grain boundaries observed in Fig. 7. e) In contrast, domains almost perpendicular to the stretching direction are probably the evidences of sealed microfractures. Misorientation angles lower and higher than  $10^\circ$  are represented with white and blue boundaries respectively.

Therefore, even if subsidiary with respect to pressure solution, quartz plasticity and recrystallization are also observed in the Hyuga Tectonic Mélange.

### 5.1.2. Foliated Morotsuka

Compared to Hyuga Tectonic Mélange, deformed quartz veins from the Foliated Morotsuka are characterized by a much larger extent of recrystallization. Inside quartz veins, equant grains of size  $\sim 10 \mu\text{m}$  (Figs. 9c–d and 12a) develop ubiquitously at the expense of parent grains. These microstructures are comparable to the ‘core-and-mantle’

structures, proposed by White (1976) and Fitz Gerald and Stünitz (1993) and also described by Urai et al. (1991) for greenschist metamorphic facies. The boundary of relict grains is sutured and show locally bulging of the recrystallized domain, as well as the incipient formation of internal subgrains (Fig. 12c), suggesting a recrystallization controlled mostly by the motion of grain boundaries (bulging) and progressive subgrain rotation. Besides, CPO analyses with a  $c$ -axes maximum parallel to Z (Fig. 12b) reflects the activation of the basal system in the (a) direction (Schmid and Casey, 1986), similarly to the shear zones observed in Hyuga Tectonic Mélange. Similar fabrics have also been observed in



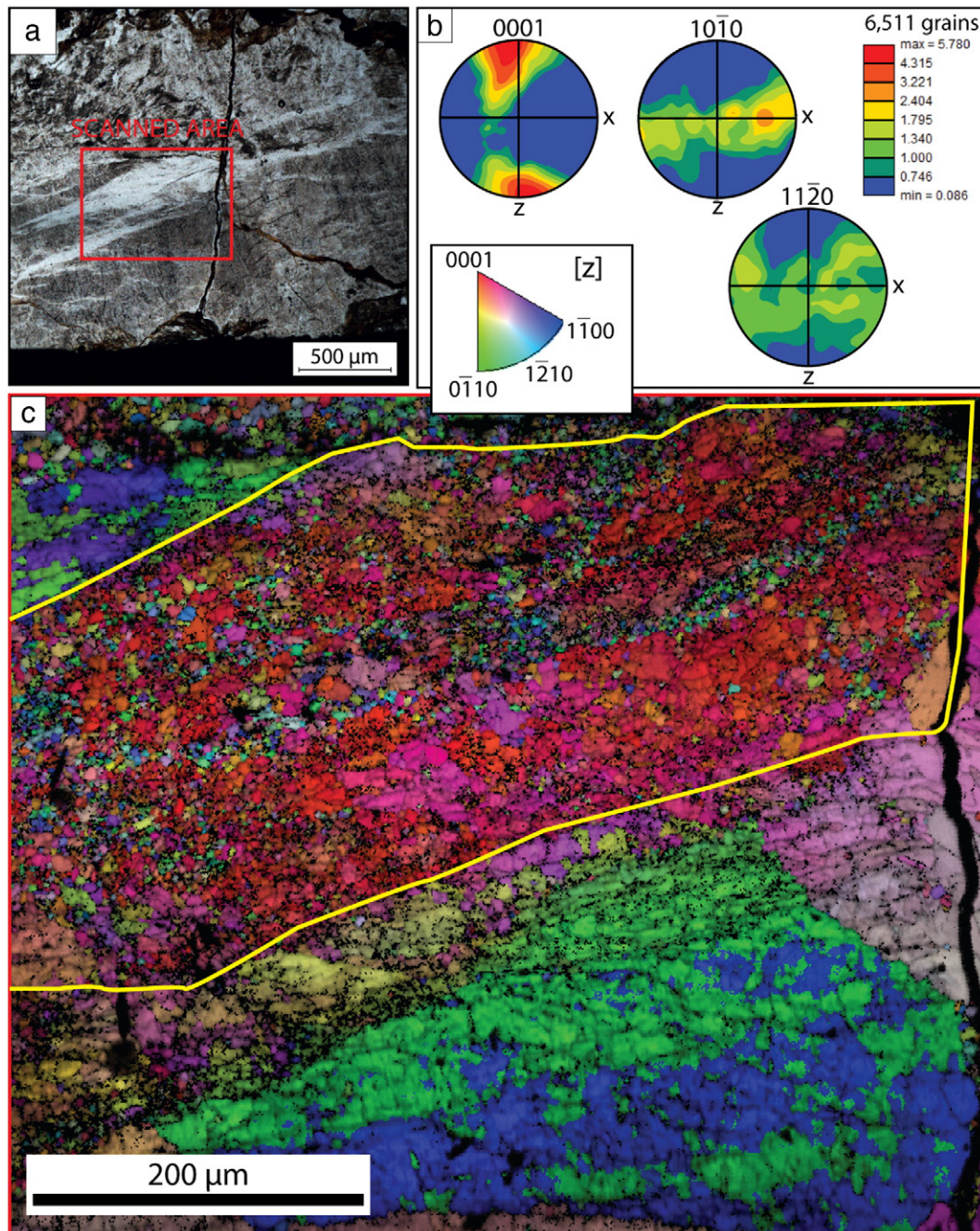


**Fig. 11.** Quartz crystallographic fabrics in a shear band in the Hyuga Tectonic Mélange. a) Optical microscope image of the scanned area. b) Lower hemisphere pole figure of  $c(0001)$  and  $a(10-10)$  axes and  $m(11-20)$ -planes corresponding to the area highlighted by the yellow polygon in c). Note the strong  $c$ -axis maxima in  $Z$  direction (normal to the foliation plane). c) EBSD map of the shear zone (with a color code associated to inverse pole figure of  $Z$  direction), showing the preferential orientation of  $c$ -axes close to the  $Z$ -direction.

natural quartz in low-grade metamorphic rocks by Schmid (1982); Hippertt (1994); Stipp et al. (2002); Trepmann and Stoekherth (2009).

In the experimental deformation framework defined by Hirth and Tullis (1992), the microstructures from Foliated Morotsuka can be associated to the transition from the dislocation creep “Regime 1” to “Regime 2”. Following these authors, at this transitional regime, recrystallization occurs predominantly by bulging of new grains and progressive subgrain rotation. However, in natural samples, these microstructures are usually ascribed to higher metamorphic conditions (Hirth and Tullis, 1992). This is thus in contrast with the estimated temperatures for the Foliated Morotsuka (Table 2), temperatures at which quartz plasticity is supposed to be only incipient. As demonstrated by experimental deformation of quartz aggregates, small amount of

water-added to the samples (e.g. Hirth and Tullis, 1992; den Brok and Spiers, 1991; Gleason and Tullis, 1995) can strongly weaken the quartz and promote recrystallization. We therefore interpret the activation of quartz plasticity at low-temperature as the result of the large water concentration in the quartz.

### 5.2. Rheological envelopes based on natural microstructures

The comparison of deformation microstructures recorded in the Hyuga Tectonic Mélange and Foliated Morotsuka provides clues to the evolution of quartz deformation mechanisms with increasing temperature near the brittle-ductile transition. Below  $\sim 300$  °C, quartz plasticity is only locally activated and pressure solution creep is the dominant



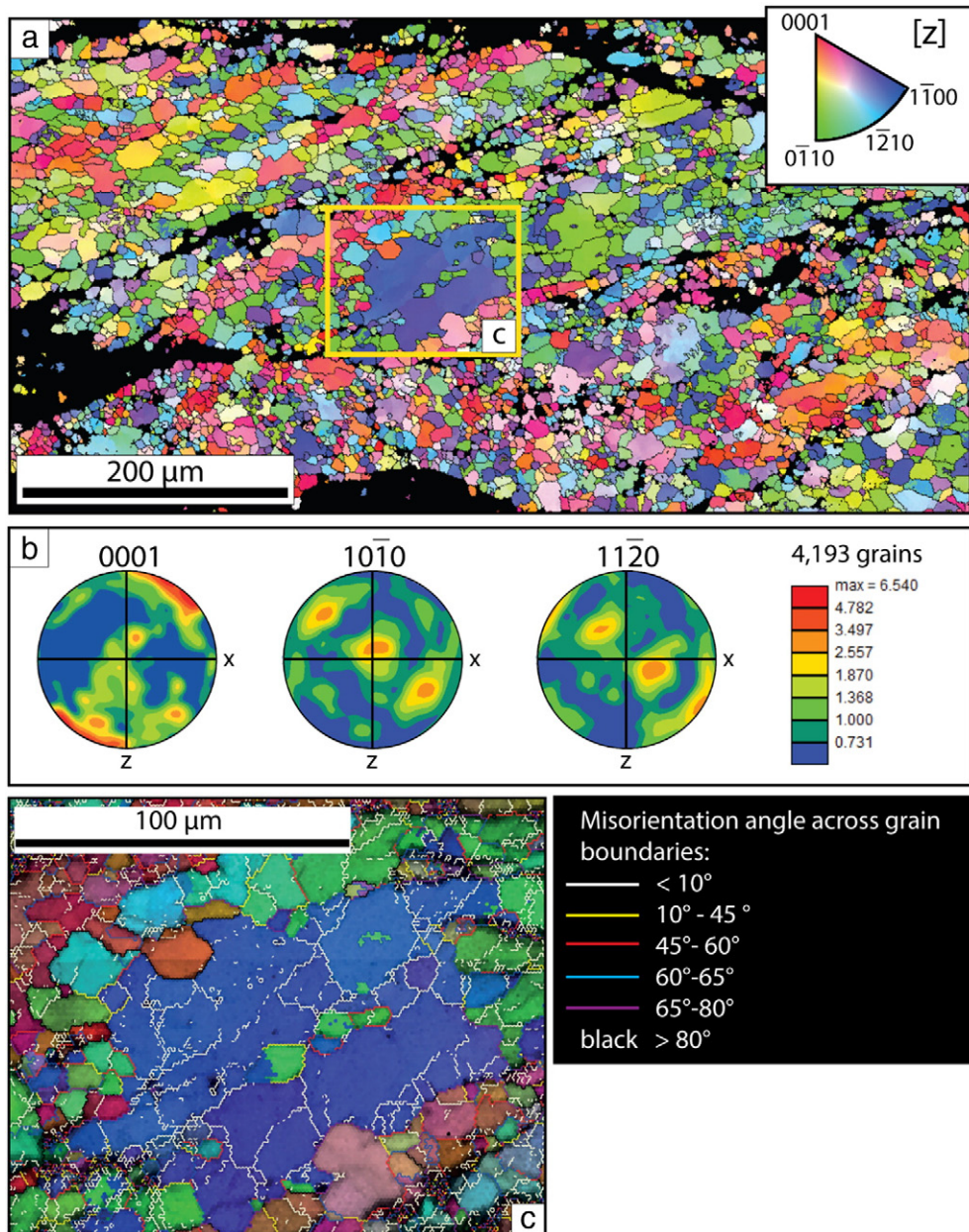


**Fig. 12.** Quartz crystallographic fabrics in a deformed vein in the Foliated Morotsuka. a) EBSD map of the quartz vein (with a color code associated to inverse pole figure of Z direction). b) Lower hemisphere pole figure c (0001) and a (10-10) axes and m (11-20)-planes of the whole map. c) Close-up view of the yellow rectangle in a). Grain boundaries are colored according to misorientation angle across the boundary. The relict blue grain shows evidences of bulging (see brown grain in upper left part) and initial stages of internal recrystallization.

deformation process for quartz. Above  $\sim 300$  °C, quartz plasticity is fully activated and controls its rheology. The temperature of this transition is relatively low, probably as a result of the very large water content of the material considered.

Then, to build rheological envelopes from quartz deformation mechanisms requires the key assumption that quartz rheology controls the bulk flow laws. This is not intuitive, as Hyuga Tectonic Mélange contains a pervasive network of phyllosilicate-rich shear zones, which can be observed at all scales and which are presumably weaker than quartz (Figs. 2 and 3). A closer look at the meter-scale shear zones shows that they are mostly discontinuous, i.e. they terminate in the matrix, and curved. This geometry implies that slip on the shear zones involves a large component of matrix deformation. Then, at smaller-scale (Fig. 3), the matrix itself is heterogeneous, constituted of small shear zones and quartz-rich boudins. Just like at larger-scale, small-scale shear zones are curved and terminate along quartz-rich sandstones blocks or ribbons. The

deformation of the matrix itself involves therefore the deformation of quartz domains, as illustrated by quartz ribbons necked at the termination of phyllosilicate-rich shear zones (Fig. 3). The geometry of the structures and microstructures in Hyuga Tectonic Mélange, typical of rocks deformed along the plate interface, supports therefore the construction of rheological envelopes on the basis of quartz mechanical behavior.

#### 5.2.1. Pressure solution creep

Pressure solution consists of the three following processes: dissolution, mass transfer and precipitation. In this sequence, the slowest of the three mechanisms imposes its kinetics to the whole system, becoming the “rate-limiting process” that controls the total strain rate (Gratier et al., 2009, Kawabata et al., 2007). Two regimes have been proposed, either controlled by the dissolution or by the diffusion of elements (Gratier et al., 2009). The boundary between the two régimes is not

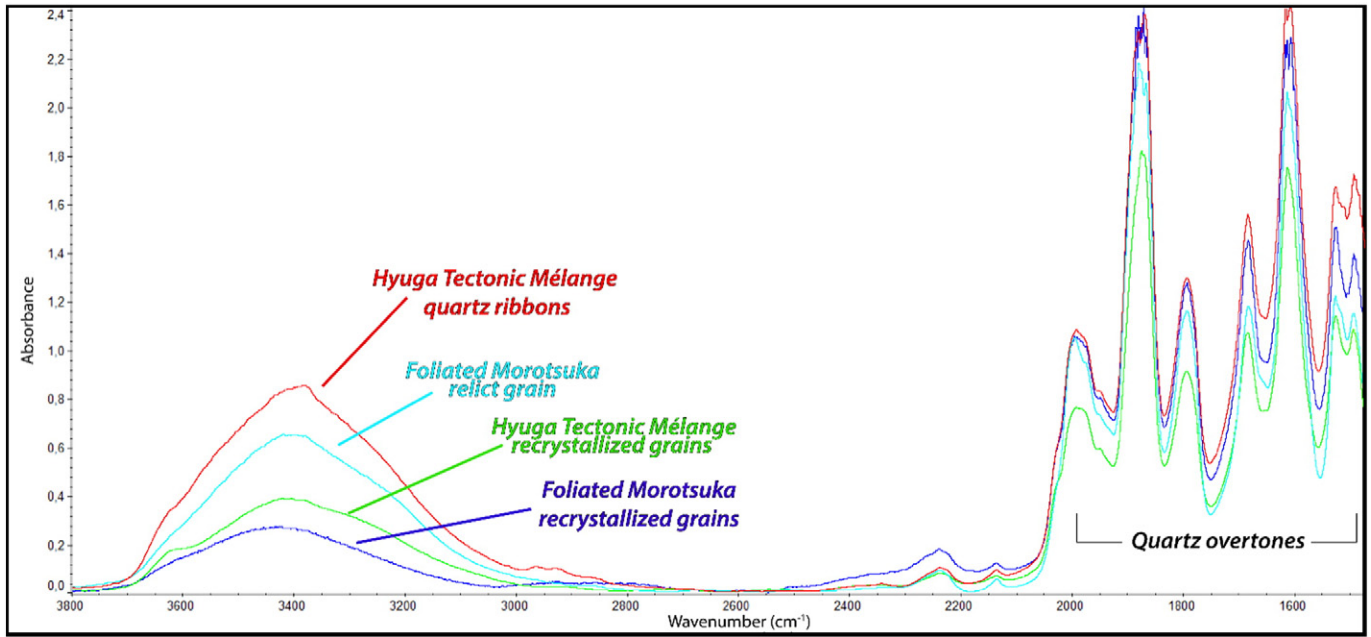


**Fig. 13.** Characteristic FTIR spectra for quartz ribbons (red) and recrystallized grains in shear bands (green) in Hyuga Tectonic Mélange and relict (cyan) and recrystallized grains (blue) in quartz veins in Foliated Morotsuka. Si—O vibrations are the 7 peaks from 2000 to 1400  $\text{cm}^{-1}$ .

easily investigable, because these processes, active at very low strain rates, are difficult to reproduce in laboratory (Gratier et al., 2009).

A major factor in determining the rate-limiting process is the physical state of the material. It has been shown that, in granular material containing a fluid saturated in quartz, dissolution acts as limiting process at the grain contacts, for temperature in the range of 150–600 °C (e.g. compaction tests (Schutjens, 1991; Dewers and Hajash, 1995; Niemeijer et al., 2002) or shearing experiments (Tenthorey and Cox, 2006)). In contrast, in non-granular samples, diffusion is the mass transport inhibitor (e.g., Rutter and Mainprice, 1979; Gratier et al., 2009). Kawabata et al. (2009) provided evidences for diffusion as rate-limiting process in sheared rocks from Shimanto accretionary complex by estimating the activation energy for pressure solution for shear-dominated rocks. The obtained values, in the order of 18  $\text{kJ mol}^{-1}$ , are in agreement with experimentally derived activation energies by Rutter and Elliott (1976) (e.g., 15  $\text{kJ mol}^{-1} \text{K}^{-1}$ ) for diffusion-controlled process, while dissolution-limited process has much higher activation energy (e.g., ~90  $\text{kJ mol}^{-1} \text{K}^{-1}$  by Gratz et al. (1990)).

On the basis of the arguments above, we assume that the relevant régime for pressure solution in the Hyuga rocks is the diffusion-limited one. We consider the creep law proposed by Gratier et al. (2009), tested by experiments with an indenter for the range of conditions in the upper to middle crust, expressed by the equation:

$$\dot{\epsilon} = D w C V_s \left( e^{\tau+3V_s/RT} - 1 \right) / d^3 \quad (3)$$

where  $\dot{\epsilon}$  is the strain rate,  $D$  is the diffusion constant along the stressed interface ( $\text{m}^2 \text{s}^{-1}$ ),  $w$  is the theoretical thickness of the fluid film (m) along which diffusion occurs,  $C$  is the solubility of quartz ( $\text{mol m}^{-3}$ ),  $V_s$  is molar volume of the solid,  $R$  the gas constant ( $8314 \text{ m}^3 \text{ Pa mol}^{-1} \text{K}^{-1}$ ),  $T$  is the temperature (K). The factor 3 in the exponential term is due to average stress across surfaces contact (Rutter and Elliott, 1976; Shimizu, 1995; Dewers and Ortoleva, 1990). The distance of mass transfer,  $d$ , strongly depending on source-sink path (Gratier et al., 2009) is very important because it controls the kinetic of diffusion creep. In compaction experiments, this value is normally the diameter of grains but, considering a non-granular material (as a foliated rock) the mean mass-transfer distance can be considered as fracture spacing (Gratier et al., 2009, 2011) or as the distance from dissolution to precipitation sites, i.e. in our case from the matrix to the ribbons. We thus chose the mean spacing between adjacent quartz ribbons in the Hyuga Tectonic Mélange, with typical distances of 1 mm ( $d_1$ ) or 500  $\mu\text{m}$  ( $d_{0.5}$ ), as representative for  $d$ . These distances have been used to estimate shear stress reported in Fig. 14. Note that these values correspond to upper bounds in stress, as considering spacing between adjacent fractures as the average transport distance  $d$  would have resulted in much smaller distances (see for example Fig. 6), hence much lower stress.

### 5.2.2. Dislocation creep

To account for the plastic deformation of quartz, incipient at  $T \sim 250$  °C in Hyuga Tectonic Mélange and fully activated at  $T \sim 340$  °C in Foliated

**Table 2**  
Molecular water content in Hyuga Tectonic Mélange (HTM) and Foliated Morotsuka (FM).

Unit	Sample	Microstructure	N of analysis	Integrated area ( $\text{cm}^{-1}$ )	Sample thickness (cm)	Water content <sup>a</sup> (H/10 <sup>6</sup> Si)	Water content <sup>b</sup> (H/10 <sup>6</sup> Si)
HTM	298	Ribbons	22	307	0,0126	19,790	20,431
HTM	HN77	Shear band	12	208	0,0130	12,977	13,417
FM	285A-3	Relict grains	35	271	0,0127	17,442	17,893
FM	285A-4	Recrystallized grains	84	47	0,0131	2,916	3008

<sup>a</sup> Absorption coefficient by Kats (1962).

<sup>b</sup> Absorption coefficient by Paterson (1982).



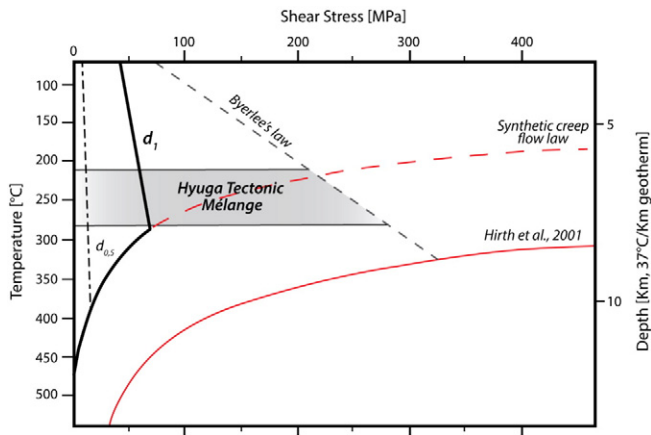


**Fig. 14.** Rheological envelope of a subduction zone, integrating pressure solution creep of quartz. Temperature gradient is assumed as  $\sim 37^\circ\text{C}/\text{km}$  (Kondo et al., 2005). The pressure solution curves are estimated with the two end-member distances of 1 mm ( $d_1$  - black dotted line) and 500  $\mu\text{m}$  ( $d_{0.5}$  - thick black lines) (see text for more details) and at constant strain rate of  $\sim 10^{-11} \text{ s}^{-1}$ . The estimated shear stress values are strongly lower than the classical Byerlee's law. Shear stresses predicted at plate interface are thus in good agreement with estimates derived from geophysical methods and thermal models ( $\sim 10$  to 35 MPa). The creep law of Hirth et al. (2001) (red line) is "too strong" to account for the onset plastic deformation in Hyuga samples. A softer, hypothetical creep flow law is proposed, in agreement with a temperature for the brittle-plastic transition in Shimanto metasediments around  $300^\circ\text{C}$  (dashed red line).

Morotsuka, we consider a classical quartz dislocation creep flow law of the form:

$$\dot{\epsilon} = A \tau^n \exp(-Q/RT) \quad (4)$$

where  $A$  is the pre-exponential number ( $\text{MPa}^{-n} \text{ s}^{-1}$ ),  $\tau$  is shear stress (MPa),  $n$  is the power law stress exponent,  $R$  the gas constant ( $8314 \text{ J mol}^{-1} \text{ K}^{-1}$ ),  $T$  is the temperature (K).

Quartz flow laws are extrapolated from laboratory experiments conducted on both natural, e.g. Simpson, Black Hills and Heavitree quartzite (Jaoul et al., 1984; Koch et al., 1989; Gleason and Tullis, 1995) or synthetic quartzites (Paterson and Luan, 1990; Luan and Paterson, 1992) in which grain size and water content are well constrained. In the light of the large water content in subduction zone meta-sediments, we considered only flow laws involving hydrated quartz. The creep flow law with the formalism proposed by Hirth et al. (2001) is probably the most appropriate to represent the quartz from the Shimanto accretionary complex because it considers explicitly the effect of water through a fugacity term ( $f$  (MPa)) (with the exponent  $m = 1$ ). However, this is a rough approximation because water quantities in experiments behind this law are two orders of magnitude lower than for quartz ribbons and parent grains in Hyuga Tectonic Mélange and Foliated Morotsuka.

### 5.2.3. Strain rate evaluations

A coarse strain rate estimate along subduction plate interface can be obtained considering the relative plate velocity and the width of the shear zone (e.g. Fagereng et al., 2010). The assumption that the sheared top-to-SE metasediments of Hyuga Tectonic Mélange were accreted at plate boundary interface (Raimbourg et al., 2014) allowed to a direct strain rate estimation considering i) the plate convergence rate and ii) the thickness of the deformation zone. Paleo reconstructions of the migration of the Pacific plate with respect to the Eurasian plate during the Early Middle Eocene (Maruyama and Send, 1986; Saito, 2008) indicate converging rates of 7,1 cm/y and 5,8 cm/y (Maruyama and Send, 1986). The thickness of the deformation zone at plate boundary corresponds to  $\sim 100$  m as estimated by field observations for the Hyuga Tectonic Mélange

(Raimbourg et al., 2014). This value is also in the range of plate-interface faults thicknesses proposed in the compilation of Rowe et al. (2013), estimated as 100 to 500 m at depth of 10–12 km. As a result, estimated strain rates are of the order  $\sim 10^{-11} \text{ s}^{-1}$ .

### 5.2.4. Strength profiles in subduction zones

We built strength profiles (Fig. 14) taking into account both pressure solution and dislocation creep for quartz at strain rates of  $10^{-11} \text{ s}^{-1}$ . As attested by incipient shear zones in Hyuga Tectonic Mélange, the onset of plastic deformation in Hyuga, must occur for temperatures below  $300^\circ\text{C}$ . The Hirth et al. (2001) creep flow law for quartz, although it is based for part on naturally deformed samples, predicts the onset of plastic deformation in the T-range  $400$ – $450^\circ\text{C}$ , at strain rates of  $10^{-11} \text{ s}^{-1}$ , while the transition is observed in Shimanto rocks around  $300^\circ\text{C}$ . A more relevant flow law should be "softer" and intersect pressure solution creep flow laws around  $300^\circ\text{C}$  (Fig. 14).

A possible strength profile, respecting all the natural constraints described above, is shown as a thick line in Fig. 14. Considering conservatively the mean transport distance of 1 mm, the effective shear stress decreases of several tens of MPa with respect to Byerlee's predictions, never exceeding 70 MPa (light grey area). Such low shear strength values are in relative agreement with shear stress magnitude at plate interface deduced from geophysical methods, e.g. from surface heat flow measurements (Peacock, 1996) or from temporal change in the stress field after mega-earthquake (e.g. Hasegawa et al., 2012), in the range of 5–30 MPa (e.g. Wintsch et al., 1995).

## 6. Summary and conclusion

The Hyuga Tectonic Mélange, deformed along the plate interface at temperatures of  $245 \pm 30^\circ\text{C}$ , provides the opportunity to investigate deformation mechanisms close to the brittle-ductile transition in subduction zones. From microscopic observation and textural analysis we showed that pressure solution coupled to micro-fracturing is the dominant quartz deformation process for this temperature. As phyllosilicate-rich shear zones generally terminate on quartz domains, bulk rheology can be estimated using quartz behavior. The consideration of pressure solution creep in rheological envelopes results in strongly reducing plate interface strength. Furthermore, plastic flow laws for quartz overestimate stress, probably because subducting metasediments are extremely rich in water hence very weak.

## Acknowledgements

This work has received funding from (i) the European Research Council (ERC) under the seventh Framework Program of the European Union (ERC Advanced Grant, grant agreement No 290864, RHEOLITH) and (ii) the Labex VOLTAIRE (ANR-10-LABX-100-01). Thin and thick sections were prepared by Gabriel Badin and Sylvain Janiec. We thank W.M.Behr and an anonymous reviewer for their help in improving this manuscript.

## References

- Aines, R.D., Rossman, G.R., 1984. Water in minerals? A peak in the infrared. *J. Geophys. Res. Solid Earth* 89, 4059–4071. <http://dx.doi.org/10.1029/JB089iB06p04059>.
- Becker, A., 1995. Quartz pressure solution: influence of crystallographic orientation. *J. Struct. Geol.* 17, 1395–1405. [http://dx.doi.org/10.1016/0191-8141\(95\)00035-C](http://dx.doi.org/10.1016/0191-8141(95)00035-C).
- Bell, T.H., Cuff, C., 1989. Dissolution, solution transfer, diffusion versus fluid flow and volume loss during deformation/metamorphism. *J. Metamorph. Geol.* 7, 425–447. <http://dx.doi.org/10.1111/j.1525-1314.1989.tb00607.x>.
- Beysac, O., Goffé, B., Chopin, C., Rouzaud, J.N., 2002. Raman spectra of carbonaceous material in metasediments: a new geothermometer. *J. Metamorph. Geol.* 20, 859–871. <http://dx.doi.org/10.1046/j.1525-1314.2002.00408.x>.
- Blanpied, M.L., Lockner, D.A., Byerlee, J.D., 1991. Fault stability inferred from granite sliding experiments at hydrothermal conditions. *Geophys. Res. Lett.* 18, 609–612. <http://dx.doi.org/10.1029/91GL00469>.
- Brander, L., Svahnberg, H., Piazolo, S., 2012. Brittle-plastic deformation in initially dry rocks at fluid-present conditions: transient behaviour of feldspar at mid-crustal

- levels. *Contrib. Mineral. Petrol.* 163, 403–425. <http://dx.doi.org/10.1007/s00410-011-0677-5>.
- Burov, E.B., 2011. Rheology and strength of the lithosphere. *Mar. Pet. Geol.* 28, 1402–1443. <http://dx.doi.org/10.1016/j.marpetgeo.2011.05.008>.
- Chester, F.M., 1988. The brittle-ductile transition in a deformation-mechanism map for halite. *Tectonophysics* 154 (1–2), 125–136. [http://dx.doi.org/10.1016/0040-1951\(88\)90230-2](http://dx.doi.org/10.1016/0040-1951(88)90230-2).
- Chester, F.M., 1995. A rheologic model for wet crust applied to strike-slip faults. *J. Geophys. Res.* 100, 13033. <http://dx.doi.org/10.1029/95JB00313>.
- Cosgrove, J.W., 1993. The interplay between fluids, folds and thrusts during the deformation of a sedimentary succession. *The Geometry of Naturally Deformed Rocks. J. Struct. Geol.* 15, pp. 491–500. [http://dx.doi.org/10.1016/0191-8141\(93\)90143-X](http://dx.doi.org/10.1016/0191-8141(93)90143-X).
- Cox, S.F., 1987. Antitaxial crack-seal vein microstructures and their relationship to displacement paths. *J. Struct. Geol.* 9, 779–787. [http://dx.doi.org/10.1016/0191-8141\(87\)90079-4](http://dx.doi.org/10.1016/0191-8141(87)90079-4).
- Cox, S.F., Etheridge, M.A., 1983. Crack-seal fibre growth mechanisms and their significance in the development of oriented layer silicate microstructures. *Deformation Processes in Tectonics. Tectonophysics* 92, pp. 147–170. [http://dx.doi.org/10.1016/0040-1951\(83\)90088-4](http://dx.doi.org/10.1016/0040-1951(83)90088-4).
- Cox, S.F., Etheridge, M.A., 1989. Coupled grain-scale dilatancy and mass transfer during deformation at high fluid pressures: examples from Mount Lyell, Tasmania. *J. Struct. Geol.* 11, 147–162. [http://dx.doi.org/10.1016/0191-8141\(89\)90040-0](http://dx.doi.org/10.1016/0191-8141(89)90040-0).
- den Brok, S.W.J., 1998. Effect of microcracking on solution-precipitation strain rate: the Gratz grain-boundary model. *Geology* 26, 915–918. [http://dx.doi.org/10.1130/0091-7613\(1998\)026<0915:EOMOPS-2.3.CO;2](http://dx.doi.org/10.1130/0091-7613(1998)026<0915:EOMOPS-2.3.CO;2).
- den Brok, S.W.J., Spiers, C.J., 1991. Experimental evidences for water weakening of quartzite by microcracking plus solution-precipitation creep. *J. Geol. Soc.* 148, 541–548. <http://dx.doi.org/10.1144/gsjgs.148.3.0541>.
- Dewers, T., Hajash, A., 1995. Rate laws for water-assisted compaction and stress-induced water-rock interaction in sandstones. *J. Geophys. Res. Solid Earth* 100, 13093–13112. <http://dx.doi.org/10.1029/95JB00912>.
- Dewers, T., Ortoleva, P., 1990. A coupled reaction/transport/mechanical model for intergranular pressure solution, stylolites, and differential compaction and cementation in clean sandstones. *Geochim. Cosmochim. Acta* 54, 1609–1625. [http://dx.doi.org/10.1016/0016-7037\(90\)90395-2](http://dx.doi.org/10.1016/0016-7037(90)90395-2).
- Durney, D.W., 1972. Solution-transfer, an important geological deformation mechanism. *Nature* 235, 315–317. <http://dx.doi.org/10.1038/235315a0>.
- Evans, J.P., 1988. Deformation mechanisms in granitic rocks at shallow crustal levels. *J. Struct. Geol.* 10, 437–443. [http://dx.doi.org/10.1016/0191-8141\(88\)90031-4](http://dx.doi.org/10.1016/0191-8141(88)90031-4).
- Fabbri, O., Faure, M., Charvet, J., 1990. Back-thrusting in accretionary prisms: microtectonics evidences from the Cretaceous–Lower Tertiary Shimanto belt of southwest Japan. *J. SE Asian Earth Sci.* 4 (3), 195–201.
- Fagereng, A., Remitti, F., Sibson, R.H., 2010. Shear veins observed within anisotropic fabric at high angles to the maximum compressive stress. *Nat. Geosci.* 3, 482–485. <http://dx.doi.org/10.1038/ngeo898>.
- Fagereng, A., Remitti, F., Sibson, R.H., 2011. Incrementally developed slickenfibers – geological record of repeating low stress-drop seismic events? *Tectonophysics* 510, 381–386. <http://dx.doi.org/10.1016/j.tecto.2011.08.015>.
- Festa, A., Pini, G.A., Dilek, Y., Codegone, G., 2010. Melanges and melange-forming processes; a historical overview and new concepts. *Int. Geol. Rev.* 52, 1040–1105. <http://dx.doi.org/10.1080/00206810903557704>.
- Fitz Gerald, J.D., Stünitz, H., 1993. Deformation of granitoids at low metamorphic grade. I: reactions and grain size reduction. *Tectonophysics* 221, 269–297. [http://dx.doi.org/10.1016/0040-1951\(93\)90163-E](http://dx.doi.org/10.1016/0040-1951(93)90163-E).
- Fukuchi, R., Fujimoto, K., Kameda, J., Hamahashi, M., Yamaguchi, A., Kimura, G., Hamada, Y., Hashimoto, Y., Kitamura, Y., Saito, S., 2014. Changes in illite crystallinity within an ancient tectonic boundary thrust caused by thermal, mechanical, and hydrothermal effects: an example from the Nobeoka Thrust, southwest Japan. *Earth Planets Space* 66, 1–12. <http://dx.doi.org/10.1186/1880-5981-66-116>.
- Gleason, G.C., Tullis, J., 1995. A flow law for dislocation creep of quartz aggregates determined with the molten salt cell. *Tectonophysics* 247, 1–23. [http://dx.doi.org/10.1016/0040-1951\(95\)00011-B](http://dx.doi.org/10.1016/0040-1951(95)00011-B).
- Goldstein, A., Knight, J., Kimball, K., 1998. Deformed graptolites, finite strain and volume loss during cleavage formation in rocks of the taconic slate belt, New York and Vermont, U.S.A. *J. Struct. Geol.* 20, 1769–1782. [http://dx.doi.org/10.1016/S0191-8141\(98\)00083-2](http://dx.doi.org/10.1016/S0191-8141(98)00083-2).
- Goldstein, A., Pickens, J., Klepeis, K., Linn, F., 1995. Finite strain heterogeneity and volume loss in slates of the Taconic Allocthon, Vermont, U.S.A. *J. Struct. Geol.* 17, 1207–1216. [http://dx.doi.org/10.1016/0191-8141\(95\)00022-6](http://dx.doi.org/10.1016/0191-8141(95)00022-6).
- Goodwin, L.B., Wenk, H.-R., 1990. Intracrystalline folding and cataclasis in biotite of the Santa Rosa mylonite zone: HVEM and TEM observations. *Tectonophysics* 172, 201–214. [http://dx.doi.org/10.1016/0040-1951\(90\)90030-C](http://dx.doi.org/10.1016/0040-1951(90)90030-C).
- Gratier, J.P., 1987. Pressure solution-deposition creep and associated tectonic differentiation in sedimentary rocks. *Geol. Soc. Lond. Spec. Publ.* 29, 25–38. <http://dx.doi.org/10.1144/GSL.SP.1987.029.01.03>.
- Gratier, J.P., 1993. Le Fluage des roches par dissolution-cristallisation sous contrainte, dans la croûte supérieure. *Bull. Soc. Geol. Fr.* 164, 267–287.
- Gratier, J.P., Gamond, J.F., 1990. Transition between seismic and aseismic deformation in the upper crust. *Geol. Soc. Lond. Spec. Publ.* 54, 461–473. <http://dx.doi.org/10.1144/GSL.SP.1990.054.01.42>.
- Gratier, J.P., Guiguet, R., Renard, F., Jenatton, L., Bernard, D., 2009. A pressure solution creep law for quartz from indentation experiments. *J. Geophys. Res.* 114. <http://dx.doi.org/10.1029/2008JB005652>.
- Gratier, J.P., Richard, J., Renard, F., Mittemperger, S., Doan, M.L., Di Toro, G., Hadizadeh, J., Boullier, A.M., 2011. Aseismic sliding of active faults by pressure solution creep; evidence from the San Andreas Fault Observatory at Depth. *Geol. Boulder* 39, 1131–1134. <http://dx.doi.org/10.1130/G32073.1>.
- Gratz, A.J., Bird, P., Quiro, G., 1990. Dissolution of quartz in aqueous basic solution, 106–236 °C: surface kinetics of “perfect” crystallographic face. *Geochim. Cosmochim. Acta* 54, 2911–2922.
- Hara, H., Kimura, K., 2008. Metamorphic and cooling history of the Shimanto accretionary complex, Kyushu, Southwest Japan: implications for the timing of out-of-sequence thrusting. *Island Arc* 17, 546–559. <http://dx.doi.org/10.1111/j.1440-1738.2008.00636.x>.
- Hasegawa, A., Yoshida, K., Asano, Y., Okada, T., Iinuma, T., Ito, Y., 2012. Change in stress field after the 2011 great Tohoku-Oki earthquake. *Earth Planet. Sci. Lett.* 355–356, 231–243. <http://dx.doi.org/10.1016/j.epsl.2012.08.042>.
- Hippert, J.F., 1994. Microstructures and c-axis fabrics indicative of quartz dissolution in sheared quartzites and phyllonites. *Tectonophysics* 229, 141–163. [http://dx.doi.org/10.1016/0040-1951\(94\)90026-4](http://dx.doi.org/10.1016/0040-1951(94)90026-4).
- Hirth, G., Tullis, J., 1992. Dislocation creep regimes in quartz aggregates. *J. Struct. Geol.* 14, 145–159. [http://dx.doi.org/10.1016/0191-8141\(92\)90053-Y](http://dx.doi.org/10.1016/0191-8141(92)90053-Y).
- Hirth, G., Teysier, C., Dunlap, J.W., 2001. An evaluation of quartzite flow laws based on comparisons between experimentally and naturally deformed rocks. *Int. J. Earth Sci.* 90, 77–87. <http://dx.doi.org/10.1007/s005310000152>.
- Hyndman, R.D., Yamano, M., Oleskevich, D.A., 1997. The seismogenic zone of subduction thrust faults. *Island Arc* 6, 244–260. <http://dx.doi.org/10.1111/j.1440-1738.1997.tb00175.x>.
- Imai, I., Teraoka, Y., Okumura, K., 1971. Geologic structure and metamorphic zonation of the northeastern part of the Shimanto terrane in Kyushu, Japan. *Chishitsugaku Zasshi J. Geol. Soc. Jpn.* 77, 207–220.
- Ito, Y., Nakashima, S., 2002. Water distribution in low-grade siliceous metamorphic rocks by micro-FTIR and its relation to grain size: a case from the Kanto Mountain region. *Jpn. Chem. Geol.* 189, 1–18. [http://dx.doi.org/10.1016/S0009-2541\(02\)00022-0](http://dx.doi.org/10.1016/S0009-2541(02)00022-0).
- Jaou, O., Tullis, J., Kronenberg, A., 1984. The effect of varying water contents on the creep behavior of Heavitree quartzite. *J. Geophys. Res. Solid Earth* 89, 4298–4312. <http://dx.doi.org/10.1029/JB089iB06p04298>.
- Kats, A., 1962. Hydrogen in alpha quartz. *Philips Res. Rep.* 17 (1–31; 133–195; 201–279).
- Kawabata, K., Tanaka, H., Kimura, G., 2007. Mass transfer and pressure solution in deformed shale of accretionary complex: examples from the Shimanto Belt, southwestern Japan. *J. Struct. Geol.* 29, 697–711. <http://dx.doi.org/10.1016/j.jsg.2006.11.009>.
- Kawabata, K., Tanaka, H., Kitamura, Y., Ma, K.-F., 2009. Apparent activation energy and rate-limiting process estimation from natural shale deformed by pressure solution in shallow subduction zone. *Earth Planet. Sci. Lett.* 287, 57–63. <http://dx.doi.org/10.1016/j.epsl.2009.07.032>.
- Kerrich, R., Beckinsale, R.D., Durham, J.J., 1977. The transition between deformation regimes dominated by intercrystalline diffusion and intracrystalline creep evaluated by oxygen isotope thermometry. *Tectonophysics* 38, 241–257. [http://dx.doi.org/10.1016/0040-1951\(77\)90213-X](http://dx.doi.org/10.1016/0040-1951(77)90213-X).
- Kirby, S.H., 1983. Rheology of the lithosphere. *Rev. Geophys. Space Phys.* 21 (6), 1458–1487. <http://dx.doi.org/10.1029/RC021i06p01458>.
- Koch, P.S., Christie, J.M., Ord, A., George, R.P., 1989. Effect of water on the rheology of experimentally deformed quartzite. *J. Geophys. Res. Solid Earth* 94, 13975–13996. <http://dx.doi.org/10.1029/JB094iB10p13975>.
- Kohlstedt, D.L., Evans, B., Mackwell, S.J., 1995. Strength of the lithosphere: constraints imposed by laboratory experiments. *J. Geophys. Res. Solid Earth* 100, 17587–17602. <http://dx.doi.org/10.1029/95JB01460>.
- Kondo, H., Kimura, G., Masago, H., Ohmori-Ikehara, K., Kitamura, Y., Ikesawa, E., Sakaguchi, A., Yamaguchi, A., Okamoto, S.-y., 2005. Deformation and fluid flow of a major out-of-sequence thrust located at seismogenic depth in an accretionary complex: Nobeoka Thrust in the Shimanto Belt, Kyushu, Japan. *Tectonics* 24, TC6008. <http://dx.doi.org/10.1029/2004TC001655>.
- Kronenberg, A.K., Tullis, J., 1984. Flow strengths of quartz aggregates: grain size and pressure effects due to hydrolytic weakening. *J. Geophys. Res. Solid Earth* 89, 4281–4297. <http://dx.doi.org/10.1029/JB089iB06p04281>.
- Kronenberg, A.K., Wolf, G.H., 1990. Fourier transform infrared spectroscopy determinations of intragranular water content in quartz-bearing rocks: implications for hydrolytic weakening in the laboratory and within the earth. *Tectonophysics* 172, 255–271. [http://dx.doi.org/10.1016/0040-1951\(90\)90034-6](http://dx.doi.org/10.1016/0040-1951(90)90034-6).
- Kronenberg, A.K., Kirby, S.H., Pinkston, J., 1990a. Basal slip and mechanical anisotropy of biotite. *J. Geophys. Res. Solid Earth* 95, 19257–19278. <http://dx.doi.org/10.1029/JB095iB12p19257>.
- Kronenberg, A.K., Segall, P., Wolf, G.H., 1990b. Hydrolytic weakening and penetrative deformation within a natural shear zone. *Geophys. Monogr.* 56, 21–36.
- Labaupe, P., Berty, C., Laurent, P., 1991. Syn-diagenetic evolution of shear structures in superficial nappes: an example from the Northern Apennines (NW Italy). *J. Struct. Geol.* 13, 385–398. [http://dx.doi.org/10.1016/0191-8141\(91\)90012-8](http://dx.doi.org/10.1016/0191-8141(91)90012-8).
- Lahfid, A., Beyssac, O., Deville, E., Negro, F., Chopin, C., Goffé, B., 2010. Evolution of the Raman spectrum of carbonaceous material in low-grade metasediments of the Glarus Alps (Switzerland). *Terra Nova* 22, 354–360. <http://dx.doi.org/10.1111/j.1365-3121.2010.00956.x>.
- Le Hebel, F., Gapais, D., Fourcade, S., Capdevila, R., 2002. Fluid-assisted large strains in a crustal-scale décollement (Hercynian Belt of South Brittany, France). *Geol. Soc. Lond. Spec. Publ.* 200, 85–101. <http://dx.doi.org/10.1144/GSL.SP.2001.200.01.06>.
- Luan, F.C., Paterson, M.S., 1992. Preparation and deformation of synthetic aggregates of quartz. *J. Geophys. Res. Solid Earth* 97, 301–320. <http://dx.doi.org/10.1029/91JB01748>.
- Maruyama, S., Send, T., 1986. Orogeny and Relative Plate Motions: Example of the Japanese Islands. *Tectonophysics, Tectonics of the Eurasian Fold Belts* 127 pp. 305–329. [http://dx.doi.org/10.1016/0040-1951\(86\)90067-3](http://dx.doi.org/10.1016/0040-1951(86)90067-3).
- Mukoyoshi, H., Hirono, T., Hara, H., Sekine, K., Tsuchiya, N., Sakaguchi, A., Soh, W., 2009. Style of fluid flow and deformation in and around an ancient out-of-sequence thrust:

- an example from the Nobeoka Tectonic Line in the Shimanto accretionary complex, Southwest Japan. *Island Arc* 18, 333–351. <http://dx.doi.org/10.1111/j.1440-1738.2009.00670.x>.
- Murata, A., 1991. Duplex structures of the Uchinohae Formation in the Shimanto Terrane, Kyushu, Southwest Japan. *J. Geol. Soc. Jpn.* 97, 39–52.
- Murata, A., 1997. Geological map of Miyazaki prefecture, 1:200,000, Miyazaki Prefectural Government.
- Murata, A., 1998. Duplexes and low-angle nappe structures of the Shimanto terrane, southwest Japan (in Japanese with English abstract). *Mem. Geol. Soc. Jpn.* 50, 147–158.
- Niemeijer, A.R., Spiers, C.J., Bos, B., 2002. Compaction creep of quartz sand at 400–600 °C: experimental evidence for dissolution-controlled pressure solution. *Earth Planet. Sci. Lett.* 195, 261–275. [http://dx.doi.org/10.1016/S0012-821X\(01\)00593-3](http://dx.doi.org/10.1016/S0012-821X(01)00593-3).
- Nishi, H., 1988. Structural analysis of the Shimanto Accretionary Complex, Kyushu, Japan, based on foraminiferal biostratigraphy. *Tectonics* 7, 641–652. <http://dx.doi.org/10.1029/T007i003p00641>.
- Paterson, M.S., 1982. The determination of hydroxyl by infrared absorption in quartz, silicate glasses and similar materials. *Bull. Mineral.* 105, 20–29.
- Paterson, M.S., Luan, F.C., 1990. Quartzite rheology under geological conditions. *Geol. Soc. Lond. Spec. Publ.* 54, 299–307. <http://dx.doi.org/10.1144/GSLSP.1990.054.01.26>.
- Peacock, S.M., 1996. Thermal and petrologic structure of subduction zones. In: *Bebout, G.E., Scholl, D.W., Kirby, S.H., Platt, J.P. (Eds.), Subduction Top to Bottom. American Geophysical Union*, pp. 119–133.
- Post, A., Tullis, J., 1998. The rate of water penetration in experimentally deformed quartzite: implications for hydrolytic weakening. *Tectonophysics* 295, 117–137. [http://dx.doi.org/10.1016/S0040-1951\(98\)00145-0](http://dx.doi.org/10.1016/S0040-1951(98)00145-0).
- Raimbourg, H., Augier, R., Famin, V., Gadenne, L., Palazzin, G., Yamaguchi, A., Kimura, G., 2014. Long-term evolution of an accretionary prism: the case study of the Shimanto Belt, Kyushu, Japan. *Tectonics* 33. <http://dx.doi.org/10.1002/2013TC003412>.
- Raimbourg, H., Vacelet, M., Ramboz, C., Famin, V., Augier, R., Palazzin, G., Yamaguchi, A., Kimura, G., 2015. Fluid circulation in the depths of accretionary prisms; an example of the Shimanto Belt, Kyushu, Japan. *Tectonophysics* 655, 161–176. <http://dx.doi.org/10.1016/j.tecto.2015.05.023>.
- Raj, R., 1982. Creep in polycrystalline aggregates by matter transport through a liquid phase. *J. Geophys. Res. Solid Earth* 87, 4731–4739. <http://dx.doi.org/10.1029/JB087iB06p04731>.
- Ramsay, J.G., 1967. *Folding and Fracturing of Rocks*. Mc-Gray Hill, New York (ed).
- Rowe, C.D., Moore, J.C., Remitti, F., the IODP Expedition 343/343T Scientists, 2013. The thickness of subduction plate boundary faults from the seafloor into the seismogenic zone. *Geology* 41, 991–994. <http://dx.doi.org/10.1130/G34556.1>.
- Rutter, E.H., 1986. On the nomenclature of mode of failure transitions in rocks. *Tectonophysics* 122, 381–387. [http://dx.doi.org/10.1016/0040-1951\(86\)90153-8](http://dx.doi.org/10.1016/0040-1951(86)90153-8).
- Rutter, E.H., Elliott, D., 1976. The kinetics of rock deformation by pressure solution (and discussion). *Philos. Trans. R. Soc. Lond. Math. Phys. Eng. Sci.* 283, 203–219. <http://dx.doi.org/10.1098/rsta.1976.0079>.
- Rutter, E.H., Mainprice, D.H., 1979. On the possibility of slow fault slip controlled by a diffusive mass transfer process. *Gerlands Beitr. Geophys.* 88, 154–162.
- Saito, M., 1996. Geological Map of Japan, 1:50,000, Geol. Surv. Jpn., Shiibamura.
- Saito, M., 2008. Rapid evolution of the Eocene accretionary complex (Hyuga Group) of the Shimanto terrane in southeastern Kyushu, southwestern Japan. *Island Arc* 17, 242–260. <http://dx.doi.org/10.1111/j.1440-1738.2008.00615.x>.
- Sakai, T., et al., 1984. Microfossil stratigraphy of the Paleogene system in Kyushu Shimanto Belt. In: *Saito, T., et al. (Eds.), Biostratigraphy and International Correlation of the Paleogene System in Japan. Yamagata Univ., Yamagata, Japan*, pp. 95–112 (in Japanese with English abstract).
- Schmid, S.M., 1982. Microfabric Studies as Indicators of Deformation Mechanisms and Flow Laws Operative in Mountain Building. *Acad. Press : London, United Kingdom*, pp. 95–110.
- Schmid, S.M., Casey, M., 1986. Complete fabric analysis of some commonly observed quartz C-axis patterns. In: *Hobbs, B.E., Heard, H.C. (Eds.), Mineral and Rock Deformation: Laboratory Studies. American Geophysical Union Monograph* vol. 36, pp. 263–286.
- Scholz, C.H., 1988. The brittle-plastic transition and the depth of seismic faulting. *Geol. Rundsch.* 77, 319–328. <http://dx.doi.org/10.1007/BF01848693>.
- Schutjens, P.M.T.M., 1991. Experimental compaction of quartz sand at low effective stress and temperature conditions. *J. Geol. Soc.* 148, 527–539. <http://dx.doi.org/10.1144/gsjgs.148.3.0527>.
- Shimizu, I., 1995. Kinetics of pressure solution creep in quartz: theoretical considerations. Influence of Fluids on Deformation Processes in Rocks. *Tectonophysics* 245, pp. 121–134. [http://dx.doi.org/10.1016/0040-1951\(94\)00230-7](http://dx.doi.org/10.1016/0040-1951(94)00230-7).
- Spiers, C.J., Schutjens, P.M.T.M., Brzesowsky, R.H., Peach, C.J., Liezenberg, J.L., Zwart, H.J., 1990. Experimental determination of constitutive parameters governing creep of rocksalt by pressure solution. *Geol. Soc. Lond. Spec. Publ.* 54, 215–227. <http://dx.doi.org/10.1144/GSLSP.1990.054.01.21>.
- Spiers, J., De Meer, S., Niemeijer, A.R., Zhang, X., 2004. Kinetics of rock deformation by pressure solution and the role of thin aqueous films. In: *Nakashima, S., et al. (Eds.), Physicochemistry of Thin Film Water. Universal Academy Press, Inc., Tokyo, Japan*, pp. 129–158.
- Stallard, A., Shelley, D., 1995. Quartz c-axes parallel to stretching directions in very low-grade metamorphic rocks. *Tectonophysics* 249, 31–40. [http://dx.doi.org/10.1016/0040-1951\(95\)00040-T](http://dx.doi.org/10.1016/0040-1951(95)00040-T).
- Stipp, M., Stünitz, H., Heilbronner, R., Schmid, S.M., 2002. The eastern Tonale fault zone: a “natural laboratory” for crystal plastic deformation of quartz over a temperature range from 250 to 700 °C. *J. Struct. Geol.* 24, 1861–1884. [http://dx.doi.org/10.1016/S0191-8141\(02\)00035-4](http://dx.doi.org/10.1016/S0191-8141(02)00035-4).
- Stöckhert, B., Gerya, T.V., 2005. Pre-collisional high pressure metamorphism and nappe tectonics at active continental margins: a numerical simulation: high pressure metamorphism and nappe tectonics. *Terra Nova* 17, 102–110. <http://dx.doi.org/10.1111/j.1365-3121.2004.00589.x>.
- Taira, A., Katto, J., Tashiro, M., Okamura, M., Kodama, K., 1988. The Shimanto Belt in Shikoku, Japan; evolution of Cretaceous to Miocene accretionary prism. *Mod. Geol.* 12, 5–46.
- Taira, A., Okada, J., Whitaker, H.M.D., Smith, A.J., 1982. The Shimanto Belt of Japan: Cretaceous-lower Miocene active margin sedimentation. In: *Leggett, J.K. (Ed.), Trench-Forearc Geology. Geol.Soc. London, Special Publication* 10, pp. 5–26.
- Tenthorey, E., Cox, S.F., 2006. Cohesive strengthening of fault zones during the interseismic period: an experimental study. *J. Geophys. Res. Solid Earth* 111, B09202. <http://dx.doi.org/10.1029/2005JB004122>.
- Teraoka, Y., Imai, I., Okumura, K., 1981. Geological Map of Japan, 1:200,000, Geol. Surv. Jpn, Nobeoka.
- Teraoka, Y., Okumura, K., 1992. Tectonic division and Cretaceous sandstone compositions of the Northern Belt of the Shimanto Terrane, southwest Japan. *Mem. Geol. Soc. Jpn.* 38, 261–270.
- Toriumi, M., Teruya, J., 1988. Tectono-metamorphism of the Shimanto Belt. *Mod. Geol.* 12, 303–324.
- Treppmann, C.A., Stoeckhert, B., 2009. Microfabric of folded quartz veins in metagreywackes; dislocation creep and subgrain rotation at high stress. *J. Metamorph. Geol.* 27, 555–570. <http://dx.doi.org/10.1111/j.1525-1314.2009.00842.x>.
- Tse, S.T., Rice, J.R., 1986. Crustal earthquake instability in relation to the depth variation of frictional slip properties. *J. Geophys. Res.* 91, 9452–9472. <http://dx.doi.org/10.1029/JB091iB09p09452>.
- Tullis, J., Yund, R.A., 1977. Experimental deformation of dry westerly granite. *J. Geophys. Res.* 82, 5705–5718. <http://dx.doi.org/10.1029/JB082i036p05705>.
- Tullis, J., Yund, R.A., 1980. Hydrolytic weakening of experimentally deformed Westerly granite and Hale albite rock. *J. Struct. Geol.* 2, 439–451. [http://dx.doi.org/10.1016/0191-8141\(80\)90005-X](http://dx.doi.org/10.1016/0191-8141(80)90005-X).
- Urai, J.L., Williams, P.F., van Roermund, H.L.M., 1991. Kinematics of crystal growth in syntectonic fibrous veins. *J. Struct. Geol.* 13, 823–836. [http://dx.doi.org/10.1016/0191-8141\(91\)90007-6](http://dx.doi.org/10.1016/0191-8141(91)90007-6).
- White, S.H., 1976. The effects of strain on the microstructures, fabrics and deformation mechanisms in quartz. *Philos. Trans. R. Soc. Lond.*, A 283, 69–86.
- Wintsch, R.P., Christoffersen, R., Kronenberg, A.K., 1995. Fluid-rock reaction weakening of fault zones. *J. Geophys. Res.* 100 (B7), 13021–13032. <http://dx.doi.org/10.1029/94JB02622>.
- Wintsch, R.P., Yi, K., 2002. Dissolution and replacement creep: a significant deformation mechanism in mid-crustal rocks. *Micro Structural Processes: A Special Issue in Honor of the Career Contributions of R.H. Vernon. J. Struct. Geol.*, 24, pp. 1179–1193. [http://dx.doi.org/10.1016/S0191-8141\(01\)00100-6](http://dx.doi.org/10.1016/S0191-8141(01)00100-6).
- Wright, T.O., Henderson, J.R., 1992. Volume loss during cleavage formation in the Meguma Group, Nova Scotia, Canada. *J. Struct. Geol.* 14, 281–290.
- Wright, T.O., Platt, L.B., 1982. Pressure dissolution and cleavage in the Martinsburg shale. *Am. J. Sci.* 282, 122–135.